JCI The Journal of Clinical Investigation

Deficiency of macrophage PHACTR1 impairs efferocytosis and promotes atherosclerotic plaque necrosis

Canan Kasikara, … , Muredach P Reilly, Ira Tabas

J Clin Invest. 2021. https://doi.org/10.1172/JCI145275.

Research In-Press Preview Cardiology Cell biology

Graphical abstract

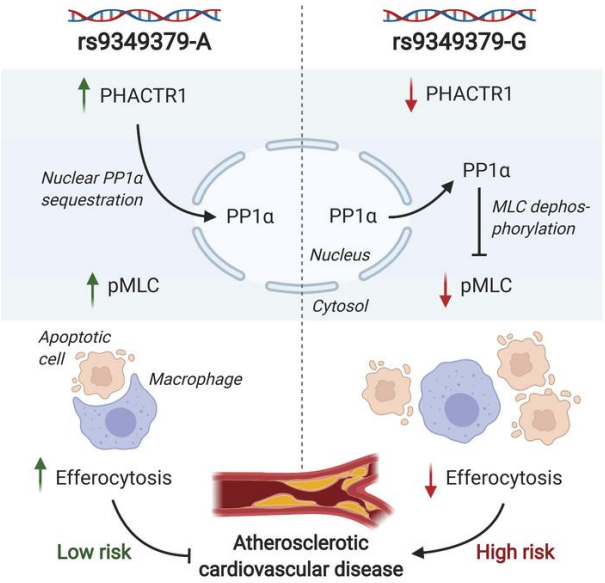

Deficiency of macrophage PHACTR1 impairs efferocytosis and promotes atherosclerotic plaque necrosis

Canan Kasikara,[1] Maaike Schilperoort,[1] Brennan Gerlach,[1] Chenyi Xue,[1] Xiaobo Wang[1], Ze Zheng,[2] George Kuriakose,[1] Bernhard Dorweiler,[3] Hanrui Zhang,[1] Gabrielle Fredman[4], Danish Saleheen,[1] Muredach P. Reilly[1,5], and Ira Tabas[1,6,7]

[1]Department of Medicine, Columbia University Irving Medical Center, New York, New York, USA. [2]Department of Medicine, Medical College of Wisconsin, Milwaukee, Wisconsin, USA. [3]Department of Vascular Surgery, University of Cologne, Cologne, Germany.[4]Deparment of Molecular and Cellular Physiology, Albany Medical Center, Albany, New York, USA. [5]Irving Institute for Clinical and Translational Research, Columbia University Irving Medical Center, New York, New York, USA. [6]Department of Physiology and Cellular Biophysics and [7]Department of Pathology and Cell Biology, Columbia University Irving Medical Center, New York, New York, USA.

Address correspondence to: Ira Tabas, Depart of Medicine, Columbia University Irving Medical Center, 630 W. 168th Street, New York, New York 10032, USA. Phone: 212.305.9430; E-mail: iat1@columbia.edu.

Abstract

Efferocytosis, the process through which apoptotic cells (ACs) are cleared through actin-mediated engulfment by macrophages, prevents secondary necrosis, suppresses inflammation, and promotes resolution. Impaired efferocytosis drives the formation of clinically dangerous necrotic atherosclerotic plaques, the underlying etiology of coronary artery disease (CAD). An intron of the gene encoding *PHACTR1* contains a common variant rs9349379 (A > G) associated with CAD. As PHACTR1 is an actin-binding protein, we reasoned that if the rs9349379 risk allele G causes lower PHACTR1 expression in macrophages, it might link the risk-allele to CAD via impaired efferocytosis. We show here that rs9349379-G/G was associated with lower levels of PHACTR1 and impaired efferocytosis in human monocyte-derived macrophages and human atherosclerotic lesional macrophages compared with rs9349379-A/A. Silencing *PHACTR1* in human and mouse macrophages compromised AC engulfment, and mice in which hematopoietic *Phactr1* was genetically targeted in Western diet-fed *Ldlr*$^{-/-}$ mice showed impaired lesional efferocytosis, increased plaque necrosis, and thinner fibrous caps—all signs of vulnerable plaques in humans. Mechanistically, PHACTR1 prevented dephosphorylation of myosin light chain (MLC), which was necessary for AC engulfment. In summary, rs9349379-G lowers PHACTR1, which, by lowering phospho-MLC, compromised efferocytosis. Thus, rs9349379-G may contribute to CAD risk, at least in part, by impairing atherosclerotic lesional macrophage efferocytosis.

Introduction

Despite the availability of safe and effective risk-reducing therapies, coronary artery disease (CAD) remains the major cause of morbidity and mortality in the United States and other developed countries (1). Ischemic CAD is caused by atherosclerosis, a lipoprotein-driven, non-resolving inflammatory process in which lipid, macrophages, other immune cells, and extracellular matrix accumulate in the arterial subendothelial space (intima) of large arteries at sites of disturbed blood flow (2-6). A distinguishing feature of clinically significant advanced atherosclerotic plaques is impaired macrophage clearance of dead cells (efferocytosis) (7-10). Impaired clearance of lesional apoptotic cells (ACs) by lesional macrophages through the process of efferocytosis promotes plaque necrosis, lesional inflammation, and defective inflammation resolution (7-10), all of which are associated with unstable atherosclerotic plaques and acute CAD (11-14). While observations in human advanced lesions and molecular-genetic causation studies in mice have supported this scenario, insight from human genetics in this area has been limited even though genome-wide association studies (GWAS) have identified many CAD-risk loci (15-21). Indeed, the application of human genetics to macrophage cell biological mechanisms in atherosclerosis remains an understudied area (18), and one of the challenges in this area is that most of the identified CAD risk loci reside in non-coding regions and have uncertain links to the genes to which they are assigned (15-21). Concerning efferocytosis, Kojima et al. (22) showed that the 9p21 CAD risk locus was associated with lower expression in smooth muscle cells of cyclin-dependent kinase inhibitor 2B (CDKN2B) and calreticulin. Calreticulin helps facilitate the recognition of ACs by macrophage LDL receptor-related protein 1 (LRP1), and the authors showed that the silencing of CDKN2B in smooth muscle cells led to decreased engulfment of apoptotic smooth muscle cells by macrophages in vitro. However, CAD risk loci that directly affect efferocytosis processes in macrophages themselves have not yet been identified.

Several independent GWAS have shown that certain intronic variants in the gene encoding phosphatase and actin regulator 1 (PHACTR1) on chromosome 6p24 are associated with CAD risk (19, 23-26). Two independent fine-mapping studies have concluded that rs9349379 (A > G), a common variant located in the 3rd intron of

PHACTR1, is the causal CAD-risk variant and that there are no secondary signals at this locus (27, 28). However, there is a discrepancy in whether *PHACTR1* is the causal gene at this locus. One prior study has suggested that the G allele at rs9349379 increases CAD risk by causing increased expression of the gene encoding endothelin-1, EDN1, in endothelial cells without affecting *PHACTR1* expression (28). However, separate work presented mechanism-based evidence that the risk variant is associated with lower expression of *PHACTR1* itself in endothelial cells (27). In particular, the variant was shown to interrupt a binding site for a transcription factor, myocyte enhancer factor-2 (MEF2), at the rs9349379 locus. Most importantly, *PHACTR1* mRNA, but not EDN1 mRNA, was found to be lower in both human endothelial cells engineered to have the rs9349379 risk variant on an isogenic background and in human coronary arteries from subjects bearing the risk variant (27, 29). Analysis of the Genotype-Tissue Expression (GTEx) dataset confirmed these eQTL data for various human arterial tissues (29, 30). Further, a recent study showed that *PHACTR1* mRNA, but not *EDN1* mRNA, is lower in human carotid atheroma versus normal carotid tissue (31). These combined data raise the possibility that the rs9349379-G risk variant may be linked to CAD through the lower expression of PHACTR1, i.e., that PHACTR1 is athero-protective. However, whether CAD risk is due to lower PHACTR1 in endothelial cells, other cell types relevant to atherosclerosis, or a combination of cell types remains to be determined. The possible role of macrophage PHACTR1 in atherosclerosis was suggested by a recent study showing that transplantation of atherosclerosis-prone *Apoe*$^{-/-}$ mice with *Phactr1*$^{-/-}$*Apoe*$^{-/-}$ bone marrow aggravated atherosclerosis (32), but possible links to the human CAD-risk polymorphism or efferocytosis remain unknown.

In this study, we investigate the hypothesis that lower expression of PHACTR1 expression in macrophages in subjects carrying the rs9349379-G allele contributes to atherosclerosis by compromising efferocytosis, specifically the ability of macrophages to internalize bound ACs. PHACTR1 contains four highly conserved RPEL domains that interact with actin and phosphatase protein 1 (PP1); and a nuclear localization signal (NLS) that facilitates PHACTR1 nuclear translocation (33-36). In NIH3T3 fibroblasts, G-actin interaction with the RPEL domains maintains PHACTR1 in the cytoplasmic, while serum-induced G-to-F-actin polymerization prevents this binding and thereby promotes

the translocation of PHACTR1 into the nucleus (36). This series of events decreases PP1 phosphatase activity in the cytoplasm, leading to increased levels of phosphorylated myosin light chain (MLC) in the cytoplasm and contraction of actinomycin complex (36). Other studies with various non-macrophage cell types have also suggested that PHACTR1 influences actin dynamics and mediates actin-mediated cell motility and membrane protrusions (37, 38), but the role of PHACTR1 in efferocytosis remains unknown. By immunohistochemistry, PHACTR1 was found to be highly expressed in macrophages in human atherosclerotic lesions, and the rs9349379 risk variant was associated with lower expression of a particular short *PHACTR1* transcript in human macrophages (39). However, the significance of this remains unknown, as this transcript, if translated, would encode a protein lacking important actin-related functional domains of PHACTR1.

Given the role of actin dynamics in efferocytosis (40), we wondered whether lower full-length PHACTR1 protein expression in lesional macrophages of rs9349379-G subjects might contribute to CAD risk by impairing efferocytosis. In support of this hypothesis, we show that both monocyte-derived macrophages and macrophages in atherosclerotic lesions of rs9349379-G/G subjects have lower expression of full-length PHACTR1 mRNA and PHACTR1 protein and impaired AC engulfment compared with rs9349379-A/A subjects. Silencing PHACTR1 in human and mouse macrophages also impaired AC engulfment, and Western diet (WD)-fed *Ldlr*$^{-/-}$ mice transplanted with *Phactr1*$^{-/-}$ or *Phactr1*$^{+/-}$ bone marrow had decreased lesional macrophage efferocytosis and increased features of plaque instability, notably increased plaque necrosis, compared with WD-fed *Phactr1*$^{+/+}$ $\rightarrow$ *Ldlr*$^{-/-}$ mice. Mechanistic data showed that the compromise in efferocytosis in *Phactr1*$^{-/-}$ macrophages is related to defective AC engulfment owing to decreased phospho-MLC secondary to increased cytoplasmic PP1α. These data support the hypothesis that lower expression of PHACTR1 in subjects with the rs9349379 risk allele contributes to atherosclerotic CAD by impairing lesional macrophage efferocytosis and thereby promoting plaque instability.

Results

Human monocyte-derived and atherosclerotic lesional macrophages carrying the rs9349379-G CAD-risk variant have lower PHACTR1 expression and impaired efferocytosis. To investigate the effect of rs9349379 risk allele on macrophage PHACTR1 expression, we used human monocyte-derived macrophages (HMDMs) obtained from anonymous New York Blood Center donors. We detected various protein isoforms of PHACTR1 in HMDMs by immunoblotting, including short (~25 kDa), intermediate (~50 kDa), and long (~75 kDa) isoforms (**Supplemental Figure 1A**). While there were no differences in the expression of the short and intermediate isoforms of PHACTR1 between the SNP carriers and non-carriers (**Supplemental Figure 1B**), there was a lower expression of *PHACTR1* mRNA and the full-length isoform of PHACTR1 protein in HMDMs carrying both copies of the CAD-risk allele (GG) vs. AA or AG, and there was a trend toward lower PHACTR1 in AG vs. AA (**Figure 1, A and B**). As noted in the Introduction, PHACTR1 encodes an actin-binding protein, which suggests a possible role in efferocytosis, as actin remodeling is a critical step in the internalization of ACs. We hypothesized that lower expression of PHACTR1 in rs9349379-GG HMDMs would lead to impaired efferocytosis, linking this risk allele to an important and established mechanism driving atherosclerosis progression and complications (7, 10, 41, 42). Accordingly, the AA, AG, and GG HMDMs were assayed for their ability to engulf PKH26-labeled ACs. The data show that efferocytosis was lower in GG HMDMs than in AA or AG HMDMs, with AG HMDMs showing a trend toward an intermediate value between GG and AA (**Figure 1C**). As PHACTR1 protein expression in the 24 AG HMDMs showed a high degree of variation, we plotted PHACTR1 expression versus efferocytosis and found a statistically significant correlation (**Figure 1D**).

As mentioned, PHACTR1 was found to be highly expressed in macrophages in human atherosclerotic lesions by immunohistochemistry (39). To gain further insight into cell-type expression of PHACTR1 in human atheroma, we used single-cell RNA-seq to examine *PHACTR1* expression in multiple cell types from a human atherosclerotic carotid artery, including macrophages and monocytes (**Supplemental Figure 2, A and B**). *PHACTR1* was among the top differentially expressed genes in macrophages (fold

change = 1.71, P-value = 3.13 x 10^{-165}) and monocytes (fold change = 3.36, P-value = 5.22 x 10^{-236}) compared with other cells. (**Supplemental Figure 2C**). The macrophage population was characterized by a high expression of FOLR2 that was shown previously to be upregulated in human atherosclerotic plaques (43) (**Supplemental Figure 2D**). This population corresponds to the “Folr2hi macrophages” reported in Lin et al. (44), which is similar to "resident-like macrophages" described by Cochain et al., which have a gene profile that overlaps partially with that of resolving-type macrophages and is distinct from two other sub-populations of lesional macrophages whose transcript profile suggests an inflammatory phenotype (45). These data raise the possibility that PHACTR1 may be particularly important in lesional macrophages that lie closer to the resolving end rather than the inflammatory end of the macrophage-phenotype spectrum.

As further support of lesional macrophage PHACTR1 expression, we found by immunofluorescence microscopic analysis of human atherosclerotic carotid arteries that most of the PHACTR1 signal colocalized with lesional $CD68^+$ macrophages (**Figure 1E**). Most importantly, this signal was lower in GG and AG plaques versus AA plaques (**Figure 1F**), while there were no significant differences in the total number of macrophages (**Figure 1G**). We then assayed these plaques for $TUNEL^+$ cells that were either associated with lesional macrophages or unassociated ("free"), the ratio of which is a reliable measure of efferocytosis in tissue specimens (46). The data show that plaques from subjects carrying one or both rs9349379-G alleles had a lower associated:free ratio, indicating relatively impaired efferocytosis (**Figure 1H**). In summary, the rs9349379-G variant, which confers higher CAD risk, tracks with lower levels of macrophage PHACTR1 and impaired efferocytosis both in vitro and in human atherosclerotic lesions.

Silencing PHACTR1 in HMDMs decreases efferocytosis and phagocytosis. To show causation between PHACTR1 and efferocytosis, HMDMs from three of the rs93749379-AA subjects in Fig. 1 were pre-treated with either scrambled RNA or siPHACTR1. The cells were incubated with or without interferon-γ (IFNγ) and lipopolysaccharide (LPS) to model inflammatory macrophages in atherosclerosis and then assayed for efferocytosis as in Figure 1C. IFNγ/LPS treatment did not change PHACTR1 expression, and we achieved good silencing with siPHACTR1 (**Figure 2, A-C**). For all three sets of HMDMs

under both basal and inflammatory conditions, PHACTR1 silencing led to impaired efferocytosis (**Figure 2, D-F**). The impairment was due to lower AC internalization, as siPHACTR1 did not lower AC binding to the macrophages (**Figure 2, G-I**). To determine if the defect in AC internalization was reflecting a general defect in phagocytosis, we tested the ability of the macrophages to internalize *E. coli* and 4-μm and 10-μm polystyrene beads. For all 3 substrates, siPHACTR1 lowered uptake by the macrophages (**Figure 2, J-K**). Thus, silencing PHACTR1 in HMDMs causes a general defect in phagocytosis, including a defect in efferocytosis.

In anticipation of the in vivo molecular and genetic causation studies in mice that follow, we assayed the role of PHACTR1 on efferocytosis in murine bone marrow-derived macrophages (BMDMs) from *Phactr1*$^{+/+}$, *Phactr1*$^{+/-}$, and *Phactr1*$^{-/-}$ mice. As with PHACTR1-silenced HMDMs, basal and IFNγ/LPS-treated BMDMs from *Phactr1*$^{+/-}$ mice showed decreased efferocytosis compared with *Phactr1*$^{+/+}$ BMDMs (**Figure 3, A and B**), and this impairment was enhanced in *Phactr1*$^{-/-}$ BMDMs (**Figure 3, C and D**). Also similar to HMDMs, PHACTR1 silencing or genetic targeting did not block AC binding to mouse BMDMs (**Figure 3E**). Finally, given the defect in AC internalization and the role of PHACTR1 as an actin-binding protein, we reasoned that PHACTR1 deficiency might alter actin remodeling around the phagocytic cup that forms around a bound AC. In support of this idea, we found that PHACTR1 silencing in BMDMs labeled with the F-actin marker LifeAct-RFP caused a defect in the formation of the typical wide-mouth actin cup around an engaged AC (**Figure 3F**). The uptake of oxidized LDL, which occurs through a mechanism independent of the actin cytoskeleton (47), was not different between *Phactr1*$^{+/+}$ and *Phactr1*$^{-/-}$ BMDMs (**Supplemental Figure 3**). In summary, silencing PHACTR1 in human and mouse macrophages causes a specific defect in the phagocytic internalization of ACs.

PHACTR1 facilitates efferocytosis by decreasing protein phosphatase-1α-mediated myosin light chain dephosphorylation. PHACTR1 mediates the assembly of stress fibers in fibroblasts by maintaining the phosphorylated, active form of myosin light chain (MLC), which facilitates actomyosin contraction (36). Given the role of actin in AC engulfment, we hypothesized that PHACTR1 enables efferocytosis by a similar mechanism. Consistent with this hypothesis, we showed that the binding of ACs to

BMDMs and HMDMs induces phosphorylation of MLC in a PHACTR1-dependent manner (**Figure 4, A and B**). Moreover, rs9349379-GG HMDMs, which have lower PHACTR1 than rs9349379-AA HMDMs, also had lower phospho-MLC (**Figure 4C**). Most importantly, silencing of MLC blocked efferocytosis in wild-type macrophages, and transfection with constitutively activated $Ser^{18,19} \rightarrow Asp^{18,19}$ MLC restored efferocytosis in PHACTR1-deficient macrophages (**Figure 4, D and E**).

MLC, a cytoplasmic protein, can be dephosphorylated by cytoplasmic PP1α but not by nuclear PP1α (48-50). In context, there is evidence in serum-stimulated fibroblasts to suggest that PHACTR1 can bind PP1α and facilitate its translocation to the nucleus in a process dependent on a nuclear localization signal (NLS) in PHACTR1 (36). To test the relevance of this pathway to macrophages carrying out efferocytosis, we conducted a series of experiments in which various factors in the pathway were genetically manipulated. First, exposure of BMDMs to ACs increased the binding of PHACTR1 to PP1α, as assessed by immunoblotting PHACTR1 in anti-PP1α immunoprecipitates (**Figure 5A**). Second, PP1α silencing increased the ratio of phospho:total MLC in both wild-type and *Phactr1*$^{-/-}$ BMDMs and, most importantly, normalized efferocytosis in *Phactr1*$^{-/-}$ macrophages (**Figure 5, B-D**). Third, exposure of BMDMs to ACs increased nuclear PHACTR1 and PP1α and decreased cytoplasmic PHACTR1 and PP1α as assessed by both immunoblot and immunofluorescence microscopy (**Figure 5, E-G**). Fourth, we studied *Phactr1*$^{-/-}$ BMDMs reconstituted with Myc-tagged wild-type PHACTR1 or PHACTR1 lacking either its NLS domain (ΔB1) or PP1α-binding domain (ΔC) (**Figure 5H**). As expected, AC-exposed *Phactr1*$^{-/-}$ macrophages transfected with the NLS-lacking ΔB1 PHACTR1 mutant showed a markedly lower nuclear:cytoplasmic ratio of PHACTR1 compared with cells reconstituted with wild-type PHACTR1 (**Figure 5I**). Moreover, reconstitution of *Phactr1*$^{-/-}$ macrophages with either of the mutant PHACTR1 forms led to a lower nuclear:cytoplasmic ratio of PP1α compared with cells reconstituted with wild-type PHACTR1 **(Figure 5J**), supporting the role of macrophage PHACTR1 in facilitating the translocation of PP1α to the nucleus. Most importantly, while reconstitution with WT PHACRT1 rescued the efferocytosis defects in *Phactr1*$^{-/-}$ BMDM, reconstitution with the mutant PHACTR1 forms lacking the NLS domain or

PP1α-binding domain failed to rescue the defective efferocytosis in *Phactr1*$^{-/-}$ BMDM (**Figure 5K**). These combined data support the hypothesis that PHACTR1 enhances MLC-mediated efferocytosis by sequestering PP1α in the nucleus and thereby preventing the dephosphorylation-deactivation of cytoplasmic MLC.

Chimeric mice lacking hematopoietic PHACTR1 show defective macrophage efferocytosis of apoptotic thymocytes. To explore the role of macrophage PHACTR1 in efferocytosis in vivo, we investigated efferocytosis in the thymuses of dexamethasone-treated mice reconstituted with *Phactr1*$^{+/+}$, *Phactr1*$^{+/-}$, or *Phactr1*$^{-/-}$ bone marrow. Dexamethasone administration causes robust thymocyte apoptosis, followed by AC clearance by thymic macrophages (51). As expected, treatment of control *Phactr1*$^{+/+}$-transplanted mice with dexamethasone caused a marked reduction in thymic weight and cellularity (**Figure 6, A and B**), which is caused by the coupled processes of thymocyte apoptosis and efferocytotic disposal of the dead cells. Accordingly, the number of annexin V$^+$ (apoptotic) cells in the thymus of these control mice showed only a slight increase (**Figure 6C**). In contrast, there was much less of a decrease in thymus weight and cellularity and a much greater increase in annexin V$^+$ and F4/80$^+$ macrophages in *Phactr1*$^{-/-}$-transplanted mice (**Figure 6, C and D**). When compared to the *Phact1*$^{+/+}$ cohort, *Phactr1*$^{+/-}$ thymuses showed slight trends toward higher thymus weight, cellularity, and ACs, but these differences did not reach statistical significance. Most importantly, the ratio of macrophage-associated:free TUNEL$^+$ cells, i.e., efferocytosis, was lower in mice reconstituted with *Phactr1*$^{+/-}$ and *Phactr1*$^{-/-}$ bone marrow (**Figure 6E**). To link these data to our mechanistic work, we assayed the ratio of` phospho:total MLC by immunofluorescence microscopy in AC-associated macrophages in the thymuses. We found that most of the positive signal for phospho-MLC was in macrophages associated with TUNEL$^+$ cells and that, as predicted by our in vitro mechanistic data, the ratio among the 3 cohorts followed the same pattern as that seen with efferocytosis (**Figure 6F**). These data provide evidence that PHACTR1 is necessary for maintaining wild-type levels of phospho-MLC and, most importantly, for enabling efficient efferocytosis in macrophages faced with a major AC challenge in vivo.

Western diet-fed Ldlr$^{-/-}$ *mice lacking hematopoietic PHACTR1 show defective macrophage efferocytosis and increased plaque necrosis in atherosclerotic lesions.*

Efferocytosis is a critical process in atherosclerosis, as efficient clearance of ACs in atherosclerotic lesions is needed to prevent the accumulation of inflammatory necrotic cells and to promote plaque-stabilizing pro-resolution processes (7, 8). Thus, as posited, defective efferocytosis could contribute to higher CAD risk in subjects carrying loss-of-expression polymorphisms in *PHACTR1*. To test this idea in experimental atherosclerosis, lethally irradiated *Ldlr*$^{-/-}$ mice were transplanted with *Phactr1*$^{+/+}$, *Phactr1*$^{+/-}$, or *Phactr1*$^{-/-}$ bone marrow and then placed on a Western-type diet for 8 weeks (*Phactr1*$^{-/-}$ *versus Phactr1*$^{+/+}$) or 12 weeks (*Phactr1*$^{+/-}$ *versus Phactr1*$^{+/+}$). Immunostaining showed that the macrophage-rich regions of the *Phactr1*$^{+/+}$ lesions expressed PHACTR1, which was less in *Phactr1*$^{+/-}$ lesions and undetectable in *Phactr1*$^{-/-}$ lesions (**Supplemental Figure 4A**). There were no significant differences in body weight, plasma cholesterol, blood glucose, plasma triglycerides, plasma lipoprotein-cholesterol profile, or blood monocytes between control and hematopoietic PHACTR1-deficient mice in either 8-week or 12-week experiments (**Supplemental Figure 4, B-G and H-M, respectively**). In both experiments, macrophage efferocytosis in aortic root atherosclerotic lesions was lower in hematopoietic PHACTR1-deficient mice compared with control mice (**Figure 7, A and D**), and this was associated with a lower phospho-MLC:total MLC ratio in lesional macrophages that were associated with TUNEL^{+} cells (**Figure 7, B and E**). Hematopoietic PHACTR1-deficient mice in both experiments caused increases in necrotic core and lesion area (**Figure 7, C and F**), and decreases in fibrous cap thickness (**Figure 7, G and H**), which is consistent with impaired resolution. In humans, plaque necrosis and thin fibrous caps are associated with plaque instability (11-13). Finally, transplantation of bone marrow from *Phactr1*$^{+/+}$ mice into *Phactr1*$^{-/-}$ *Ldlr*$^{-/-}$ recipients (*Phactr1*$^{+/+}$ $\rightarrow$ *Phactr1*$^{-/-}$ *Ldlr*$^{-/-}$ mice) caused an increase in aortic root lesional macrophage efferocytosis and a decrease in lesional necrotic area compared with the lesions of *Phactr1*$^{-/-}$ $\rightarrow$ *Phactr1*$^{-/-}$ *Ldlr*$^{-/-}$ mice (**Figure 7I**), further supporting the idea that hematopoietic PHACTR1 helps stabilize plaques. Total lesion area was also lower in the *Phactr1*$^{+/+}$ $\rightarrow$ *Phactr1*$^{-/-}$ *Ldlr*$^{-/-}$ cohort (**Supplemental Figure 5A**), while there were no significant differences between the two groups in body weight, plasma cholesterol, blood glucose, or blood monocytes (**Supplemental Figure 5, B-E, respectively**). In summary, these experimental

atherosclerosis data, when considered together with the human lesional, HMDM, and mechanistic data, add support to the hypothesis that impaired macrophage efferocytosis conferred by *PHACTR1* loss-of-expression polymorphisms contributes to a higher risk of atherosclerotic CAD.

Discussion

Defective efferocytosis and its consequences, including post-apoptotic cellular necrosis, cellular debris-mediated inflammation, and impaired resolution, are important drivers of clinically dangerous plaque features (7-10). While these studies have shown defective macrophage efferocytosis in advanced human coronary plaques, impaired efferocytosis has also been observed in macrophages derived from the circulating monocytes of CAD versus healthy patients in a manner that correlated with plaque severity (14). Among the mechanisms of defective efferocytosis in atherosclerosis are defects in one or more macrophage efferocytosis processes, i.e., AC binding, actin-mediated AC engulfment, and phagolysosomal AC degradation and processing (7-10). Concerning AC engulfment, most work has emphasized the roles of GTPases, particularly Rac1, and their cognate GTP-exchange factors, in orchestrating actin remodeling around the developing AC phagosome (52-54). The work here shows that phosphorylation-activation of MLC, mediated by sequestration of PP1α in the nucleus by PHACTR1, is also necessary for optimal AC engulfment by macrophages. To our knowledge, the role of MLC in efferocytosis has not previously been reported, but the role of myosin, particularly cortical actinomyosin, in providing the force needed to form phagosomes has been widely studied (55). Indeed, the idea that MLC/myosin plays a similar role in efferocytosis is consistent with our data in Figure 3F that PHACTR1 silencing impairs phagosome formation around an AC.

Among the many CAD-risk loci that have been identified over the last decade, the *PHACTR1* intronic rs9349379 risk allele G is notable for the reproducibility and strength of its association with CAD and its relatively high frequency (17, 19, 23). The combination of these genetic data, the role of PHACTR1 in AC engulfment elucidated here, and the critical role of impaired efferocytosis in atherosclerosis progression suggested a mechanistic hypothesis linking the risk allele to CAD. The plausibility of this

hypothesis is supported by our data linking the risk variant to lower expression of PHACTR1 in macrophages, particularly atherosclerotic lesional macrophages, which had not previously been shown in any cell type for PHACTR1 protein. The data demonstrating this point in HMDMs and human lesional macrophages may have a mechanistic basis in terms of regulation of *PHACTR1* transcription, as previous data in human endothelial cells showed that the risk variant lowered *PHACTR1* mRNA by compromising the binding of a transcription factor, myocyte enhancer factor-2 (MEF2), to a putative enhancer region in the intronic locus (27, 29). As MEF2 is also expressed in human macrophages (56), this mechanism of transcriptional repression may also applicable to macrophages. Of note, a report showing lower expression of only a short form of *PHACTR1* mRNA in HMDMs from rs9349379-GG subjects (39) is not consistent with our protein data and is discussed below.

Six transcripts have been reported to originate from the human *PHACTR1* gene: long, intermediate-A+, intermediate-A-, intermediate-B+, intermediate-B-, and short (39, 57). The long transcript encodes a 580-amino acid protein with 4 actin-binding RPEL motifs and PP1 binding domain, all of which are conserved in the protein translated from the long form of mouse *Phactr1* mRNA (33, 36). Curiously, one of the aforementioned papers reported that the long transcript of *PHACTR1* could not be detected in $CD14^+$ monocyte-derived macrophages by PCR or immunoblotting, whereas it was the short transcript that was shown to be lower in monocyte-macrophages from subjects harboring rs9349379-GG by qPCR (39), while one of the others reported that human macrophages express only the intermediate-B and short alleles by PCR, but did not look at the effect of rs9349379 genotype (57). In contrast, we were able to readily detect the long transcript by qPCR and its encoded PHACTR1 protein isoform by immunoblot in HMDMs. We also showed that the long-form expression was lower in rs9349379-GG subjects, as was immunoreactive PHACTR1 protein co-localizing with macrophage in atherosclerotic lesions. Most importantly, the presence and functional importance of the long form of PHACTR1 in macrophages is implicated by our in vitro and in vivo molecular-genetic causation studies, as it is only this form that has both the NLS and PP1α-binding domains required for the efferocytotic function of PHACTR1.

While these combined data suggest that impaired efferocytosis might be a mechanism linking the risk variant to CAD, we favor the idea that additional, complementary mechanisms are also involved, including those involving other consequences of decreased PHACTR1 in macrophages, decreased PHACTR1 in endothelial cells (27, 29, 58), and possibly increased endothelin-1 in endothelial cells (28). Regarding other possible macrophage effects, Li et al. (32) reported recently that fat-fed *Apoe*$^{-/-}$ mice with an absence of hematopoietic PHACTR1 had increased atherosclerosis compared with *Apoe*$^{-/-}$ mice. The authors ascribed this effect to the induction of an inflammatory signaling pathway in *Phactr1*$^{-/-}$ macrophages. However, as efferocytosis was not examined in this report, future studies will be needed to determine if this inflammatory pathway is a separate consequence of PHACTR1 deficiency or secondary to impaired efferocytosis, which is known to activate inflammatory pathways (59). Moreover, as neither *PHACTR1* polymorphisms nor human atheroma was examined, the potential relevance of the mouse findings in this study to human atherosclerosis and the rs9349379 risk variant remains to be investigated. In considering the role(s) of PHACTR1 in endothelial cells, the consequences of lower PHACTR1 or higher endothelin-1 in these cells could be additive or synergistic with effects in macrophages, as these two cell types play complementary and interactive roles in atherosclerosis (2). Moreover, the endothelial hypothesis may also have relevance to non-atherosclerotic vascular diseases associated with rs9349379-G, including migraine headache, arterial dissection, fibromuscular dysplasia, hypertension, and coronary microvascular dysfunction (28, 60, 61). Except for coronary microvascular dysfunction, the risk of these non-atherosclerotic vascular diseases is lower in carriers of the rs9349379-G variant in contrast to the higher risk of CAD conferred by rs9349379-G, indicating that future work is needed to link the polymorphism to these diseases.

In summary, we present new roles for PHACTR1, MLC, and PP1α in efferocytosis and show that the *PHACTR1* intronic rs9349379 CAD risk allele lowers the fully functional form of PHACTR1 protein and impairs efferocytosis in human atherosclerotic lesional macrophages and HMDMs. We also show direct causation and mechanistic evidence in hematopoietic *Phactr1*-targeted mice. When considered together with the

possible atherogenic role of PHACTR1 deficiency in lesional endothelial cells, as well as a recent study showing lower *PHACTR1* mRNA in human carotid atheroma versus normal carotid (31), our findings suggest that therapies that could enhance PHACTR1 expression, such as agonists of receptors that lead to PHACTR1 induction (37), may have promise as a new human genetics-based therapy for atherosclerosis and possibly other vascular diseases.

Methods

Cell lines. The Jurkat human T lymphocyte E6-1 cell line was obtained from ATCC and cultured in DMEM (GIBCO) supplemented with 10% (vol/vol) heat-inactivated fetal bovine serum (HI-FBS; GIBCO), 10 U/mL penicillin, and 100 mg/mL streptomycin (Corning). Cells were cultured in a humidified CO_2 incubator at 37°C.

Bone marrow-derived macrophages (BMDMs). Mice were euthanized with isoflurane, and hind legs were removed. Femurs and tibias were flushed with DMEM containing 4.5 g/l glucose (GIBCO), 20% L-929 fibroblast-conditioned media, 10% HI-FBS, and 1% penicillin/streptomycin using a 26-gauge needle. Cell suspensions were passed over a 40-μm filter, centrifuged at 500 *g*, resuspended in 50 ml of media, and plated into five 100-mm dishes. Cells were incubated for 4 days, after which non-adherent cells and debris were aspirated and the medium was replaced with fresh medium. After 7 to 10 days of differentiation, with media changed every 2 to 3 days, cells were harvested for use in various experiments.

Human monocyte-derived macrophages (HMDMs). Peripheral blood leukocytes were isolated from buffy coats of anonymous, de-identified healthy adult volunteers purchased from the New York Blood Center (NYBC), with informed consent obtained by the NYBC. In brief, the buffy coats were gently layered onto Histopaque solution (Sigma-Aldrich) and centrifuged at 1,620 g for 30 min at room temperature. Leukocytes were removed from the middle layer, washed with RPMI-1640 (GIBCO) containing 10% FBS and 1% penicillin/streptomycin, and then centrifuged at 1,620 g for 5 min. This wash step was repeated once before resuspending the pellet in RPMI-1640 media and plating cells into 12-well plates. After approximately 3 to 4 hours, when more than 50% of the cells were adherent, the medium was changed to RPMI-1640 medium

supplemented with 10 ng/ml GM-CSF (PeproTech). The medium was replaced with fresh GM-CSF-containing medium every 2 days. The macrophages were used for experiments between days 7 and 14, at which time the cells were more than 80% confluent.

Single-cell RNA-seq data analysis. Expression matrices of human atherosclerotic carotid artery single-cell RNA-seq (scRNA-seq) from three subjects were downloaded from Gene Expression Omnibus (GSE155512). The de-identified carotid artery specimens were obtained from patients undergoing carotid endarterectomy for high-grade stenosis of the internal carotid artery at Columbia University Irving Medical Center. The use of these specimens, which were removed for clinical indications only and would otherwise have been discarded, was approved by the Columbia University IRB, and procedures were conducted in accordance with an approved IRB protocol. Informed consent was obtained from each patient. Data filtering, integration, and clustering analysis were performed in Seurat 3.1.1 (62). The following gene level and cell level filtering were applied to each sample: 1) included genes expressed in ≥10 cells; 2) included cells that had 200 to 4,000 genes expressed and had ≤20,000 UMIs; 3) included cells that had ≤10% reads mapped to mitochondrial genes. Filtered datasets were integrated using SCTransform workflow. Briefly, 1,000 variable genes were selected from each dataset and the top 1,500 variable genes across three datasets were used as integration features. Integration anchors were identified using the first 20 dimensions from canonical correlation analysis. Uniform Manifold Approximation and Projection (UMAP) visualization was generated using the first 20 principal components (PC). SNN graph was constructed using 30 nearest neighbors and 20 dimensions of PCs. Louvain clustering was then performed with a resolution parameter of 0.6. Differential expression analysis was performed on cells from each cluster compared to all other cells using the MAST test implemented in Seurat, where each gene was required to be present in ≥25% of the cells in either group. A gene was considered differentially expressed if it had fold change ≥1.5 and Bonferroni corrected P-value <0.05.

Animal husbandry. Mice were socially housed in standard cages at 22^{o}C under a 12-12-hour light-dark cycle in a barrier facility with ad libitum access to water and food.

Sperm of C57BL/6NCrl-*Phactr1*$^{-/-}$ was purchased from UC Davis KOMP Repository (MMRRC:043404-UCD) and in vitro fertilization was conducted by Charles River Laboratories using C57BL/6J eggs. *Phactr1*$^{+/-}$ pups were sent to Columbia University's animal facility, where the mice were backcrossed for more than 10 generations with C57BL/6J mice (Jackson Labs, Stock No. 000664). *Phactr1*$^{+/-}$ on the C57BL/6J background were cross-bred to obtain wild-type (*Phactr1*$^{+/+}$), *Phactr1*$^{+/-}$, and *Phactr1*$^{-/-}$ mice for bone-marrow transplantation into *Ldlr*$^{-/-}$ mice (Jackson Labs, Stock No. 000227). *Ldlr*$^{-/-}$ recipient mice were randomly assigned to experimental groups by investigators. *Phactr1*$^{-/-}$ mice were crossed with *Ldlr*$^{-/-}$ mice (Jackson Labs, Stock No. 000227) to obtain *Ldlr*$^{-/-}$ *Phactr1*$^{-/-}$ as a recipient mice for bone-marrow transplantation from wild-type (*Phactr1*$^{+/+}$) and *Phactr1*$^{-/-}$ mice. Investigators were blinded for the atherosclerosis studies but were not blinded for the dexamethasone-induced thymus injury experiments.

Induction of apoptosis and fluorescent labeling of Jurkat cells. Jurkat cells were irradiated under a 254-nm UV lamp for 15 min, followed by incubation under normal cell culture conditions for 2-3 hours. The cells were then rinsed once with serum-free DMEM, resuspended at a concentration of 2 x 10^7 cells/mL in Diluent C (Sigma-Aldrich), and stained with PKH26 dye (Sigma-Aldrich) following to manufacturer's protocol. The cells were then rinsed twice with DMEM containing 10% heat-inactivated FBS and used for experiments. This method routinely typically yields > 85% annexin V^+ ACs.

LPS and IFNγ stimulation of macrophages. BMDMs from wild-type, *Phactr1*$^{+/-}$, and *Phactr1*$^{-/-}$ mice or siPHACTR1-treated HMDMs were plated at 0.2 × 10^6 cells per well on 24-well plates and allowed to adhere overnight. The following day, cells were exposed to medium containing 1 ng/ml LPS (Sigma-Aldrich) and 20 ng/ml IFNγ (PeproTech) or vehicle control. After incubating for 24 hours, the cells were either incubated with ACs to assay efferocytosis or subjected to immunoblot analysis.

In vitro efferocytosis assay. BMDMs or HMDMs were plated in 24-well dishes at a density of 0.18 X 10^6 cells per well. PKH26-labeled ACs were added to the wells at a 5:1 AC:macrophage ratio. After 45 min of incubation, the macrophage monolayers were rinsed three times with PBS and then fixed with 4% formaldehyde for 20 min, rinsed three times with PBS, and imaged on a Leica epifluorescence microscope (DMI6000B)

Dil-oxLDL uptake assay. BMDMs were plated in 24-well dishes at a density of 0.2 x 10^6 cells per well and allowed to adhere overnight. The following day, the cells were incubated with 10 μg/ml Dil-labeled oxidized LDL (Dil-oxLDL; Invitrogen). After 4 hours, cells were rinsed with PBS and fixed with 4% formaldehyde for 15 min. Cells were rinsed again, counterstained with Hoechst (1 μg/ml, Cell Signaling) for 15 min, and imaged on a Leica epifluorescence microscope (DMI6000B).

Immunoblotting and immunofluorescence microscopy of macrophages. Macrophages were lysed in 2x Laemmli lysis buffer (Bio-Rad) containing 50 mM DTT. Cell lysates were boiled for 5 min and then separated on 4–20% SDS-PAGE gradient gels (Invitrogen) at 120V for 1.5-2 hours, and electro-transferred to 0.45-mm nitrocellulose membranes at 250 amp for 1-2 hours. The membranes were incubated overnight at 4°C with 1:1000 anti-PHACTR1 (Novus, NBP1-84232 for HMDMs (Figure 1); Abcam, ab229120 for BMDMs and HMDMs (Figure 2)), anti-GAPDH (Cell Signaling, 8884S), anti-MLC (Abcam, ab79935), anti-PP1α (Abcam, ab150782), and anti-MYC (Cell Signaling, 2272S) diluted in PBS containing 1% BSA, and detected using HRP-conjugated secondary antibodies (Pierce). Densitometry was performed using ImageJ software. For immunofluorescence microscopy, macrophages were incubated with ACs at a 5:1 AC:macrophage ratio for 20 min and then fixed in 4% formaldehyde, permeabilized with 0.1% Triton X-100, blocked for 1 hour with 1% denatured bovine serum albumin (BSA), and incubated 1:100 anti-MLC2 (Abcam, ab79935), anti-P-MLC2 (Cell Signaling Technologies, #3671), anti-PHACTR1 (Abcam, ab229120), anti-PP1α (Abcam, ab150782) antibodies for at least 18 hours. Cells were rinsed with TBS with 0.1% Tween 20 (TBST) and incubated for 2 hours with 1:200 AlexaFluor-488 and AlexaFluor-647-conjugated secondary antibodies (Biolegend). Unbound secondary antibodies were removed by rinsing three times with TBST, and then the cells were incubated with Hoechst stain (1 μg/ml, Cell Signaling) for 15 min followed by another rinsing with TBST. Then cells were visualized and image-captured using a Leica epifluorescence microscope (DMI6000B).

Confocal microscopy imaging. ScrRNA or *Phactr1* siRNA were electroporated into BMDMs with 1.5 μg of LifeAct-RFP (mTagRFP-T-Lifeact-7; Addgene plasmid #54586) using the Neon Invitrogen Electroporation kit (Invitrogen). BMDMs were subjected to

1650-V at 10-millisecond intervals for 2 pulses within the electroporation chamber, then plated onto 8-well glass-bottom coverslips and allowed to adhere for 18-24 hours. ACs were then added at a 3:1 ratio of ACs:macrophages for an additional 45 min after which the macrophages were rinsed with PBS and then fixed with 4% paraformaldehyde for 15 min at room temperature. Imaging was conducted on a Zeiss LSM 880 NLO confocal microscope with an Airyscan module (Carl Zeiss Microscopy) equipped with a 63x oil 1.4 numerical aperture (NA) objective lens and collected through a 32-channel GaAsP detector as 0.2 Airy units per channel. Z-stack images were acquired at an average of 30 slices, with a 0.17-μm distance between each slice.

siRNA-mediated gene silencing. Scrambled siRNA control and gene-targeting siRNAs (Integrated DNA Technologies) were transfected into macrophages using INTERFERin® siRNA transfection reagent (Polyplus-transfection®) in 24-well plates following the manufacturer's instructions. To downregulate all isoforms of PHACTR1, a pool of siRNAs was used targeting exons 3, 14, and 15 of the human *PHACTR1* gene, or exons 11, 12, and 13 of the murine *Phactr1* gene. Cells were incubated for 6 hours with 1.5 mL of Opti-MEM (GIBCO) containing INTERFERin siRNA transfection reagent, 0.18 x 10^6 cells, and 10 nM siRNA. Experiments and protein analyses were conducted three days later.

Quantitative PCR. RNA was isolated from macrophages using the RNeasy Kit (QIAGEN), and cDNA was synthesized from RNA, which ranged from 500 ng to 1 μg per reaction, using a cDNA synthesis kit (Applied Biosystems). Real-time PCR was conducted using a 7500 Real-Time PCR System and SYBR Green reagents (Applied Biosystems). Human primer sets used were as follows: *PHACTR1* forward AGAAGAGCTGATAAAGCGAGGA; *PHACTR1* reverse TCCATGATGTCTGACGGTTGG; *HPRT* forward CCTGGCGTCGTGATTAGTGAT; and *HPRT1* reverse AGACGTTCAGTCCTGTCCATAA.

Immunoprecipitation of PP1α from macrophage nuclei. BMDMs were seeded to 100-mm culture dishes and were incubated in the presence or absence of ACs for 20 min at 37°C. Cells were removed from the dishes and added to 0.5 ml of ice-cold cytoplasmic extraction reagent of the NE-PER™ Nuclear and Cytoplasmic Extraction Kit (Thermo Fisher) and incubated on ice for 10 min. Then cell lysates were centrifuged at

14,000 x g for 5 min at 4˚C, and the pellets were resuspended with 0.25 ml of the nuclear extraction reagent of the kit and incubated for 40 min, followed by centrifugation at 14,000 x g for 10 min at 4˚C. The resulting supernatant fraction was pre-absorbed using 20 µl Protein G magnetic beads (Cell Signaling) and then incubated overnight with anti-PP1α (ThermoFisher, #43-8100) antibody while gently rotating at 4˚C. Rabbit IgG was used as a negative control. 20 µl of Protein G magnetic beads were added to the solution, and after incubation for 20 min at room temperature, the beads were collected using a magnetic rack. The beads were then rinsed five times with 500 µl cell lysis buffer (Cell Signaling), suspended in 40 µl of 4x Laemmli Sample Buffer (Bio-Rad), and subjected to immunoblot analysis.

Genotyping of rs9349379. Genomic DNA was isolated from HMDMs or carotid artery tissue using a genomic DNA extraction kit from Invitrogen per the manufacturer's instructions. DNA was genotyped using TaqMan SNPs Genotyping Assay (Thermo Fisher) for rs9349379 per the manufacturer's instructions.

Plasmids and electroporation. cDNAs for the mouse *Phactr1* and *Mlc2* genes were synthesized and cloned into the pcDNA3.1-c-Myc vector by using EcoRI and XhoI restriction enzymes (GenScript) (36). *Phactr1* mutants were derived from the pcDNA3.1-*c-Myc-Phactr1* vector by deleting B1 to delete the NLS site C to delete the PP1α-binding site (GenScript). The *Mlc2* mutant was derived from the pcDNA3.1-*c-Myc-MLC* vector by mutating S18 and S19 sites to aspartic acid. The plasmids (2 µg) were electroporated into 2 x 10^6 *Phactr1*$^{-/-}$ BMDMs (for *Phactr1* mutants) or 2 x 10^6 *Phactr1*$^{+/+}$ and *Phactr1*$^{-/-}$ BMDMs (for *Mlc2* mutant) using the Neon Transfection System from Invitrogen. Pellets of BMDMs and DNA were resuspended in 10 µl Buffer R (Invitrogen) and subjected to electroporation at 1550 V at 10-millisecond intervals for 2 pulses. Macrophages were then plated into 24-well culture dishes, and experiments and protein analyses were conducted three days later.

Blood and plasma analyses. Fasting blood glucose was measured using a glucose meter (One Touch Ultra, Lifescan) in mice that were fasted for 5 hours, with free access to water. Standard kits were used to measure plasma triglycerides (Wako, Triglyceride M Kit) and cholesterol (Wako, Cholesterol E kit) per the manufacturer's instructions.

Complete blood cell count, including leukocyte differential, was obtained using a FORCYTE Hematology Analyzer (Oxford Science).

Mouse atherosclerosis study. Eight-week-old male *Ldlr*$^{-/-}$ and *Ldlr*$^{-/-}$ *Phactr1*$^{-/-}$ mice were irradiated using 1000 rads from a 137 Cesium Gammacell source. Four hours after irradiation, the mice were injected via tail vein with 5 x 10^6 bone marrow cells from 16-20-week-old *Phactr1*$^{+/+}$ and *Phactr1*$^{-/-}$ male mice. The bone marrow cells were prepared as follows: Femurs from donor mice were isolated and flushed with DMEM containing BMDM cell medium. The cells were filtered through a 40-μm nylon cell and centrifuged at 600 g for 10 min at room temperature. Bone marrow cells were rinsed twice, and the pellets were diluted in DMEM. Mice were given water containing neomycin (0.1 mg/ml, Sigma-Aldrich) for two weeks after bone marrow transplantation (BMT). Four weeks after BMT, mice were placed on a Western diet (WD; Envigo) for 8 weeks (for the *Phactr1*$^{+/+}$ versus *Phactr1*$^{-/-}$ BMT study and the *Phactr1*$^{+/+}$ versus *Phactr1*$^{-/-}$ reverse BMT study in *Ldlr*$^{-/-}$ *Phactr1*$^{-/-}$ mice) or 16 weeks (for *Phactr1*$^{+/+}$ versus *Phactr1* $^{+/-}$ BMT study). At the time of harvest, mice were euthanized using isoflurane. Blood was removed by left ventricular puncture, and the vasculature was then perfused with cold PBS. Aortic roots were fixed in paraformaldehyde and paraffin-embedded. Serial 6-μm sections were obtained for analysis. For morphometric analysis, 6 paraffin sections 60 μm apart were stained with Harris' H&E. Total lesion and necrotic core areas were defined as previously described (63). Collagen staining was performed using picrosirius red (Polysciences) per the manufacturer's instructions. Collagen cap thickness was quantified from 3 distinct regions of the plaque as previously described (63). Sections were deparaffinized and subjected to antigen retrieval using 10 mM Tris, 0.5 M EDTA, 0.05% Tween-20. For the identification of TUNEL$^+$ cells, the TUNEL staining kit from Roche was used, using a staining period of 1 hour at 37°C. For immunostaining, sections were blocked for 1 hour using serum-free protein blocking buffer (DAKO, catalog X0909) and then incubated overnight at 4°C with the following primary antibodies: Mac2 (Cedarline, CL8942LE, 1:1000), P-MLC2 (Cell Signaling Technologies, #3671, 1:100), T-MLC2 (Abcam, ab79935, 1:100). Two slides, each with 2 sections, were assessed for each mouse. Parallel slides were used for staining with isotype controls. After rinsing in PBS, slides were incubated with secondary antibodies

for 2 hours at room temperature and were counterstained with DAPI. In situ efferocytosis was quantified as described below. Mean fluorescence intensity (MFI) of phospho-MLC was quantified in $Mac2^+$ cells that were associated with $TUNEL^+$ cells and expressed relative to total MLC MFI. All images were captured using a Zeiss fluorescence microscope and analyzed using ImageJ.

Human plaque analysis. De-identified carotid artery specimens were obtained from patients undergoing carotid endarterectomy for high-grade stenosis of the internal carotid artery at the Division of Vascular Surgery, University Medical Center, Johannes-Gutenberg University. After retrieval in the operating room, the excised plaques were rinsed in physiologic saline, immediately snap-frozen in liquid nitrogen, and then store at -80°C. After thawing, samples were fixed in 4% formalin overnight, decalcified in EDTA for 4 days, and then embedded in paraffin blocks. Serial sections were obtained at 5-µm intervals. Before immunofluorescence staining, all sections were deparaffinized in xylene and then rehydrated in a graded series of ethanol concentrations. Sections were then boiled for 20 min in an antigen retrieval buffer (10 mM Tris, 0.5 M EDTA, 0.05% Tween-20). After rinsing in PBS, sections were stained for $TUNEL^+$ cells as above. After incubating in serum-free protein blocking buffer (DAKO, catalog X0909) for 1 hour, sections were incubated overnight at 4°C with primary antibody directed toward CD68 (DAKO, catalog M0814, 1:100) for the in situ efferocytosis assay described below. For PHACTR1 staining, sections were incubated with anti-PHACTR1 antibody (Abcam, ab229120, 1:100) overnight at 4°C. The sections were then rinsed in PBS and incubated with secondary antibodies for 2 hours at room temperature. Parallel slides were used for staining with isotype controls. Slides were mounted with DAPI-containing mounting solution, and images were obtained using a Leica microscope and analyzed using FIJI/ImageJ software (NIH). Two slides, each with 2 sections, were assessed for each patient. To evaluate whether the risk allele had a primary effect on decreasing PHACTR1 expression and efferocytosis by lesional macrophages, the lesions were selected to be similarly advanced in terms of plaque necrosis, i.e., to make sure that any effects seen were not simply secondary to an effect of the risk allele on causing more advanced plaques.

In situ efferocytosis. Mouse aortic roots, human carotid arteries, or mouse thymus sections were assessed for efferocytosis by counting TUNEL$^+$ nuclei that were associated with Mac2$^+$ macrophages (‘‘associated’’), indicative of efferocytosis, or not associated with macrophages (‘‘free’’) (63). Macrophage-associated TUNEL$^+$ cells were defined as TUNEL$^+$ nuclei surrounded by or in contact with Mac2$^+$ macrophages. Free ACs exhibited nuclear condensation, loss of antibody Mac2 reactivity, and were not in contact with neighboring macrophages.

In vivo dexamethasone thymus assay. Eight-week-old male *Phactr1*$^{+/+}$, *Phactr1*$^{+/-}$, and *Phact1r*$^{-/-}$ mice were injected i.p. with 250 mL PBS containing 250 mg dexamethasone (Sigma-Aldrich) or PBS control. Eighteen hours after injection, the mice were euthanized, and thymuses were harvested and weighed. One lobe of the thymus from each mouse was mechanically disaggregated, and cells were enumerated. Flow cytometry was then conducted to determine the number of annexin V$^+$ cells. The other thymus lobe was formalin-fixed, paraffin-embedded, and sectioned, followed by staining of the sections (5mm) with TUNEL reagents (Roche) and antibodies to Mac2 (Cedarlane, CL8942LE, 1:1000), P-MLC2 (Cell Signaling Technologies,#3671, 1:100) and T-MLC2 (Abcam, ab79935, 1:100). For P-MLC2 quantification, thymus sections were stained with TUNEL reagent, anti-P-MLC2, and anti-total MLC2. Either TUNEL$^+$ ACs engulfing or contacting Mac2$^+$ cells were chosen in which MFI of P-MLC2 was measured and normalized to Mac2$^+$ cells’ total MLC MFI.

Flow cytometric analysis of apoptotic cells. Cells were washed twice with cold FACS buffer (PBS containing 2% FBS and 1 mM EDTA), resuspended in annexin V-binding buffer (Biolegend) at a concentration of 1x10^6 cells/1 ml, and incubated with FITC-conjugated annexin V (Biolegend) for 15 min at room temperature. Samples were then analyzed on a BD FACS CantoII flow cytometer. Data analysis was carried out using FlowJo software.

Quantification and statistical analysis. Data were tested for normality using the Kolmogorov-Smirnov test, and statistical significance was determined using GraphPad Prism software. Data that passed the normality test were analyzed using Student’s t-test for two groups with one variable tested and equal variances, one-way ANOVA with Dunnett’s multiple comparison test for multiple groups with only one variable tested, or

two-way ANOVA with Bonferroni post-tests for more than two groups with multiple variables tested. Data that were not normally distributed but contained equal variances were analyzed using the nonparametric Mann-Whitney U test with posthoc analysis. Data are shown as mean values ± SEM. Differences were considered statistically significant at $P < 0.05$.

Study approval. University Institutional Review Board and Health Insurance Portability and Accountability Act guidelines were followed for isolating peripheral human blood leukocytes. Mouse protocols were approved by Columbia University's institutional animal care and use committee. All mice were cared for according to the NIH guidelines for the care and use of laboratory animals, and all were in good general health based on appearance and activity. The use of de-identified carotid artery specimens, which were removed for clinical indications only and would otherwise have been discarded, conformed with the declaration of Helsinki and were approved for use by the Johannes-Gutenberg University ethics review board. Informed consent was obtained from each patient. The Columbia University IRB provided ethical approval for these studies, and procedures were conducted in accordance with an approved IRB protocol.

Author contributions

CK, DS, HZ, MPR, and IT conceived and designed the research. BD donated patient samples and was instrumental in the interpretation of the human data. CK, MS, BG, CX, XW, and GK conducted the experiments. CK, MS, BG, CX, ZZ, GF, GK, HZ, MPR, and IT analyzed the data. CK, MS, and IT wrote the paper, with comments provided by all other authors.

Acknowledgments

This work was supported by an American Heart Association post-doctoral fellowship grant 20POST35210962 (to CK), the Niels Stensen Fellowship (to MS), NIH T32 training grant HL007343-28 (to BG), an American Society of Hematology Scholar Award and an American Heart Association Career Development Award (to ZZ), NIH grant HL141127 (to GF), NIH grants R00HL130574 and R01HL151611 (to HZ), NIH grants

HL113147 and HL150359 (to MPR), and NIH R35 grant HL145228 (to IT). These studies used the resources of the Columbia Cancer Center flow core facilities, funded in part through NIH grants P30CA013696, P30CA013696, and S10RR027050. The graphical abstract was created using BioRender.

Conflict of interest

The authors have declared that no conflict of interest exists.

References

1. Virani SS, Alonso A, Benjamin EJ, Bittencourt MS, Callaway CW, Carson AP, et al. Heart disease and stroke statistics-2020 update: a report from the American Heart Association. *Circulation.* 2020;141(9):e139-e596.
2. Lusis AJ. Atherosclerosis. *Nature.* 2000;407:233-41.
3. Tabas I, Williams KJ, and Boren J. Subendothelial lipoprotein retention as the initiating process in atherosclerosis: update and therapeutic implications. *Circulation.* 2007;116(16):1832-44.
4. Glass CK, and Witztum JL. Atherosclerosis. the road ahead. *Cell.* 2001;104:503-16.
5. Kasikara C, Doran AC, Cai B, and Tabas I. The role of non-resolving inflammation in atherosclerosis. *J Clin Invest.* 2018;128(7):2713-23.
6. Libby P, and Hansson GK. Biology of disease: involvement of the immune system in human atherogenesis--current knowledge and unanswered questions. *Lab Invest.* 1991;64:5-15.
7. Yurdagul A, Jr., Doran AC, Cai B, Fredman G, and Tabas IA. Mechanisms and consequences of defective efferocytosis in atherosclerosis. *Front Cardiovasc Med.* 2017;4:86.
8. Linton MF, Babaev VR, Huang J, Linton EF, Tao H, and Yancey PG. Macrophage apoptosis and efferocytosis in the pathogenesis of atherosclerosis. *Circ J.* 2016;80(11):2259-68.
9. Schrijvers DM, De Meyer GR, Kockx MM, Herman AG, and Martinet W. Phagocytosis of apoptotic cells by macrophages is impaired in atherosclerosis. *Arterioscler Thromb Vasc Biol.* 2005;25(6):1256-61.
10. Kojima Y, Weissman IL, and Leeper NJ. The role of efferocytosis in atherosclerosis. *Circulation.* 2017;135(5):476-89.
11. Kolodgie FD, Virmani R, Burke AP, Farb A, Weber DK, Kutys R, et al. Pathologic assessment of the vulnerable human coronary plaque. *Heart.* 2004;90:1385-91.
12. Libby P. Mechanisms of acute coronary syndromes and their implications for therapy. *N Engl J Med.* 2013;368(21):2004-13.
13. Fredman G, Hellmann J, Proto JD, Kuriakose G, Colas RA, Dorweiler B, et al. An imbalance between specialized pro-resolving lipid mediators and pro-inflammatory leukotrienes promotes instability of atherosclerotic plaques. *Nat Commun.* 2016;7:12859.

14. Eligini S, Cosentino N, Fiorelli S, Fabbiocchi F, Niccoli G, Refaat H, et al. Biological profile of monocyte-derived macrophages in coronary heart disease patients: implications for plaque morphology. *Sci Rep.* 2019;9(1):8680.
15. Musunuru K, and Kathiresan S. Genetics of common, complex coronary artery disease. *Cell.* 2019;177(1):132-45.
16. McPherson R, and Tybjaerg-Hansen A. Genetics of coronary artery disease. *Circ Res.* 2016;118(4):564-78.
17. Deloukas P, Kanoni S, Willenborg C, Farrall M, Assimes TL, Thompson JR, et al. Large-scale association analysis identifies new risk loci for coronary artery disease. *Nat Genet.* 2013;45(1):25-33.
18. Howson JMM, Zhao W, Barnes DR, Ho WK, Young R, Paul DS, et al. Fifteen new risk loci for coronary artery disease highlight arterial-wall-specific mechanisms. *Nat Genet.* 2017;49(7):1113-9.
19. Nikpay M, Goel A, Won HH, Hall LM, Willenborg C, Kanoni S, et al. A comprehensive 1,000 Genomes-based genome-wide association meta-analysis of coronary artery disease. *Nat Genet.* 2015;47(10):1121-30.
20. Samani NJ, Erdmann J, Hall AS, Hengstenberg C, Mangino M, Mayer B, et al. Genomewide association analysis of coronary artery disease. *N Engl J Med.* 2007;357(5):443-53.
21. van der Harst P, and Verweij N. Identification of 64 novel genetic loci provides an expanded view on the genetic architecture of coronary artery disease. *Circ Res.* 2018;122(3):433-43.
22. Kojima Y, Downing K, Kundu R, Miller C, Dewey F, Lancero H, et al. Cyclin-dependent kinase inhibitor 2B regulates efferocytosis and atherosclerosis. *J Clin Invest.* 2014;124(3):1083-97.
23. Kathiresan S, Voight BF, Purcell S, Musunuru K, Ardissino D, Mannucci PM, et al. Genome-wide association of early-onset myocardial infarction with single nucleotide polymorphisms and copy number variants. *Nat Genet.* 2009;41(3):334-41.
24. Hager J, Kamatani Y, Cazier JB, Youhanna S, Ghassibe-Sabbagh M, Platt DE, et al. Genome-wide association study in a Lebanese cohort confirms PHACTR1 as a major determinant of coronary artery stenosis. *PLoS One.* 2012;7(6):e38663.
25. Nelson CP, Goel A, Butterworth AS, Kanoni S, Webb TR, Marouli E, et al. Association analyses based on false discovery rate implicate new loci for coronary artery disease. *Nat Genet.* 2017;49(9):1385-91.
26. Lu X, Wang L, Chen S, He L, Yang X, Shi Y, et al. Genome-wide association study in Han Chinese identifies four new susceptibility loci for coronary artery disease. *Nat Genet.* 2012;44(8):890-4.
27. Beaudoin M, Gupta RM, Won HH, Lo KS, Do R, Henderson CA, et al. Myocardial infarction-associated SNP at 6p24 interferes with MEF2 binding and associates with PHACTR1 expression levels in human coronary arteries. *Arterioscler Thromb Vasc Biol.* 2015;35(6):1472-9.
28. Gupta RM, Hadaya J, Trehan A, Zekavat SM, Roselli C, Klarin D, et al. A genetic variant associated with five vascular diseases is a distal regulator of endothelin-1 gene expression. *Cell.* 2017;170(3):522-33.e15.
29. Wang X, and Musunuru K. Confirmation of causal rs9349379- PHACTR1 expression quantitative trait locus in human-induced pluripotent stem cell endothelial cells. *Circ Genom Precis Med.* 2018;11(10):e002327.
30. Human genomics. The Genotype-Tissue Expression (GTEx) pilot analysis: multitissue gene regulation in humans. *Science.* 2015;348(6235):648-60.

31. Green IE, Williams SR, Sale MM, Keene KL, Worrall BB, and Southerland AM. Differential expression of PHACTR1 in atheromatous versus normal carotid artery tissue. *J Clin Neurosci.* 2020;74:265-7.
32. Li T, Ding L, Wang Y, Yang O, Wang S, and Kong J. Genetic deficiency of Phactr1 promotes atherosclerosis development via facilitating M1 macrophage polarization and foam cell formation. *Clin Sci (Lond).* 2020.
33. Allen PB, Greenfield AT, Svenningsson P, Haspeslagh DC, and Greengard P. Phactrs 1-4: A family of protein phosphatase 1 and actin regulatory proteins. *Proc Natl Acad Sci U S A.* 2004;101(18):7187-92.
34. Sagara J, Higuchi T, Hattori Y, Moriya M, Sarvotham H, Shima H, et al. Scapinin, a putative protein phosphatase-1 regulatory subunit associated with the nuclear nonchromatin structure. *J Biol Chem.* 2003;278(46):45611-9.
35. Mouilleron S, Wiezlak M, O'Reilly N, Treisman R, and McDonald NQ. Structures of the Phactr1 RPEL domain and RPEL motif complexes with G-actin reveal the molecular basis for actin binding cooperativity. *Structure.* 2012;20(11):1960-70.
36. Wiezlak M, Diring J, Abella J, Mouilleron S, Way M, McDonald NQ, et al. G-actin regulates the shuttling and PP1 binding of the RPEL protein Phactr1 to control actomyosin assembly. *J Cell Sci.* 2012;125(Pt 23):5860-72.
37. Allain B, Jarray R, Borriello L, Leforban B, Dufour S, Liu WQ, et al. Neuropilin-1 regulates a new VEGF-induced gene, Phactr-1, which controls tubulogenesis and modulates lamellipodial dynamics in human endothelial cells. *Cell Signal.* 2012;24(1):214-23.
38. Favot L, Gillingwater M, Scott C, and Kemp PR. Overexpression of a family of RPEL proteins modifies cell shape. *FEBS Lett.* 2005;579(1):100-4.
39. Reschen ME, Lin D, Chalisey A, Soilleux EJ, and O'Callaghan CA. Genetic and environmental risk factors for atherosclerosis regulate transcription of phosphatase and actin regulating gene PHACTR1. *Atherosclerosis.* 2016;250:95-105.
40. Poon IK, Lucas CD, Rossi AG, and Ravichandran KS. Apoptotic cell clearance: basic biology and therapeutic potential. *Nat Rev Immunol.* 2014;14(3):166-80.
41. Linton MF, Babaev VR, Huang J, Linton EF, Tao H, and Yancey PG. Macrophage Apoptosis and Efferocytosis in the Pathogenesis of Atherosclerosis. *Circ J.* 2016;80(11):2259-68.
42. Schrijvers DM, De Meyer GR, Kockx MM, Herman AG, and Martinet W. Phagocytosis of apoptotic cells by macrophages is impaired in atherosclerosis. *Arterioscler Thromb Vasc Biol.* 2005;25(6):1256-61.
43. Müller A, Beck K, Rancic Z, Müller C, Fischer CR, Betzel T, et al. Imaging atherosclerotic plaque inflammation via folate receptor targeting using a novel 18F-folate radiotracer. *Mol Imaging.* 2014;13:1-11.
44. Lin JD, Nishi H, Poles J, Niu X, McCauley C, Rahman K, et al. Single-cell analysis of fate-mapped macrophages reveals heterogeneity, including stem-like properties, during atherosclerosis progression and regression. *JCI Insight.* 2019;4(4).
45. Cochain C, Vafadarnejad E, Arampatzi P, Pelisek J, Winkels H, Ley K, et al. Single-cell RNA-Seq reveals the transcriptional landscape and heterogeneity of aortic macrophages in murine atherosclerosis. *Circ Res.* 2018;122(12):1661-74.
46. Thorp E, Cui D, Schrijvers DM, Kuriakose G, and Tabas I. Mertk receptor mutation reduces efferocytosis efficiency and promotes apoptotic cell accumulation and plaque necrosis in atherosclerotic lesions of *Apoe*-/- mice. *Arterioscler Thromb Vasc Biol.* 2008;28(8):1421-8.
47. Sun B, Boyanovsky BB, Connelly MA, Shridas P, van der Westhuyzen DR, and Webb NR. Distinct mechanisms for OxLDL uptake and cellular trafficking by class B scavenger receptors CD36 and SR-BI. *J Lipid Res.* 2007;48(12):2560-70.

48. Kaneko-Kawano T, Takasu F, Naoki H, Sakumura Y, Ishii S, Ueba T, et al. Dynamic regulation of myosin light chain phosphorylation by Rho-kinase. *PLoS One.* 2012;7(6):e39269.
49. Matsumura F, and Hartshorne DJ. Myosin phosphatase target subunit: Many roles in cell function. *Biochem Biophys Res Commun.* 2008;369(1):149-56.
50. Ito M, Nakano T, Erdodi F, and Hartshorne DJ. Myosin phosphatase: structure, regulation and function. *Mol Cell Biochem.* 2004;259(1-2):197-209.
51. Park D, Han CZ, Elliott MR, Kinchen JM, Trampont PC, Das S, et al. Continued clearance of apoptotic cells critically depends on the phagocyte Ucp2 protein. *Nature.* 2011;477(7363):220-4.
52. Elliott MR, and Ravichandran KS. The dynamics of apoptotic cell clearance. *Dev Cell.* 2016;38(2):147-60.
53. Proto JD, Doran AC, Gusarova G, Yurdagul A, Jr., Sozen E, Subramanian M, et al. Regulatory T cells promote macrophage efferocytosis during inflammation resolution. *Immunity.* 2018;49(4):666-77.e6.
54. Yurdagul A, Jr., Subramanian M, Wang X, Crown SB, Ilkayeva OR, Darville L, et al. Macrophage metabolism of apoptotic cell-derived arginine promotes continual efferocytosis and resolution of injury. *Cell Metab.* 2020;31(3):518-33.
55. Barger SR, Gauthier NC, and Krendel M. Squeezing in a meal: myosin functions in phagocytosis. *Trends Cell Biol.* 2020;30(2):157-67.
56. Aude-Garcia C, Collin-Faure V, Bausinger H, Hanau D, Rabilloud T, and Lemercier C. Dual roles for MEF2A and MEF2D during human macrophage terminal differentiation and c-Jun expression. *Biochem J.* 2010;430(2):237-44.
57. Codina-Fauteux VA, Beaudoin M, Lalonde S, Lo KS, and Lettre G. PHACTR1 splicing isoforms and eQTLs in atherosclerosis-relevant human cells. *BMC Med Genet.* 2018;19(1):97.
58. Jarray R, Pavoni S, Borriello L, Allain B, Lopez N, Bianco S, et al. Disruption of phactr-1 pathway triggers pro-inflammatory and pro-atherogenic factors: New insights in atherosclerosis development. *Biochimie.* 2015;118:151-61.
59. Lemke G, and Rothlin CV. Immunobiology of the TAM receptors. *Nat Rev Immunol.* 2008;8(5):327-36.
60. Ford TJ, Corcoran D, Padmanabhan S, Aman A, Rocchiccioli P, Good R, et al. Genetic dysregulation of endothelin-1 is implicated in coronary microvascular dysfunction. *Eur Heart J.* 2020.
61. Saw J, Yang ML, Trinder M, Tcheandjieu C, Xu C, Starovoytov A, et al. Chromosome 1q21.2 and additional loci influence risk of spontaneous coronary artery dissection and myocardial infarction. *Nat Commun.* 2020;11(1):4432.
62. Butler A, Hoffman P, Smibert P, Papalexi E, and Satija R. Integrating single-cell transcriptomic data across different conditions, technologies, and species. *Nat Biotechnol.* 2018;36(5):411-20.
63. Fredman G, Kamaly N, Spolitu S, Milton J, Ghorpade D, Chiasson R, et al. Targeted nanoparticles containing the pro-resolving peptide Ac2-26 protect against advanced atheosclerosis in hypercholesterolemic mice. *Sci Transl Med.* 2015;7:275ra20.

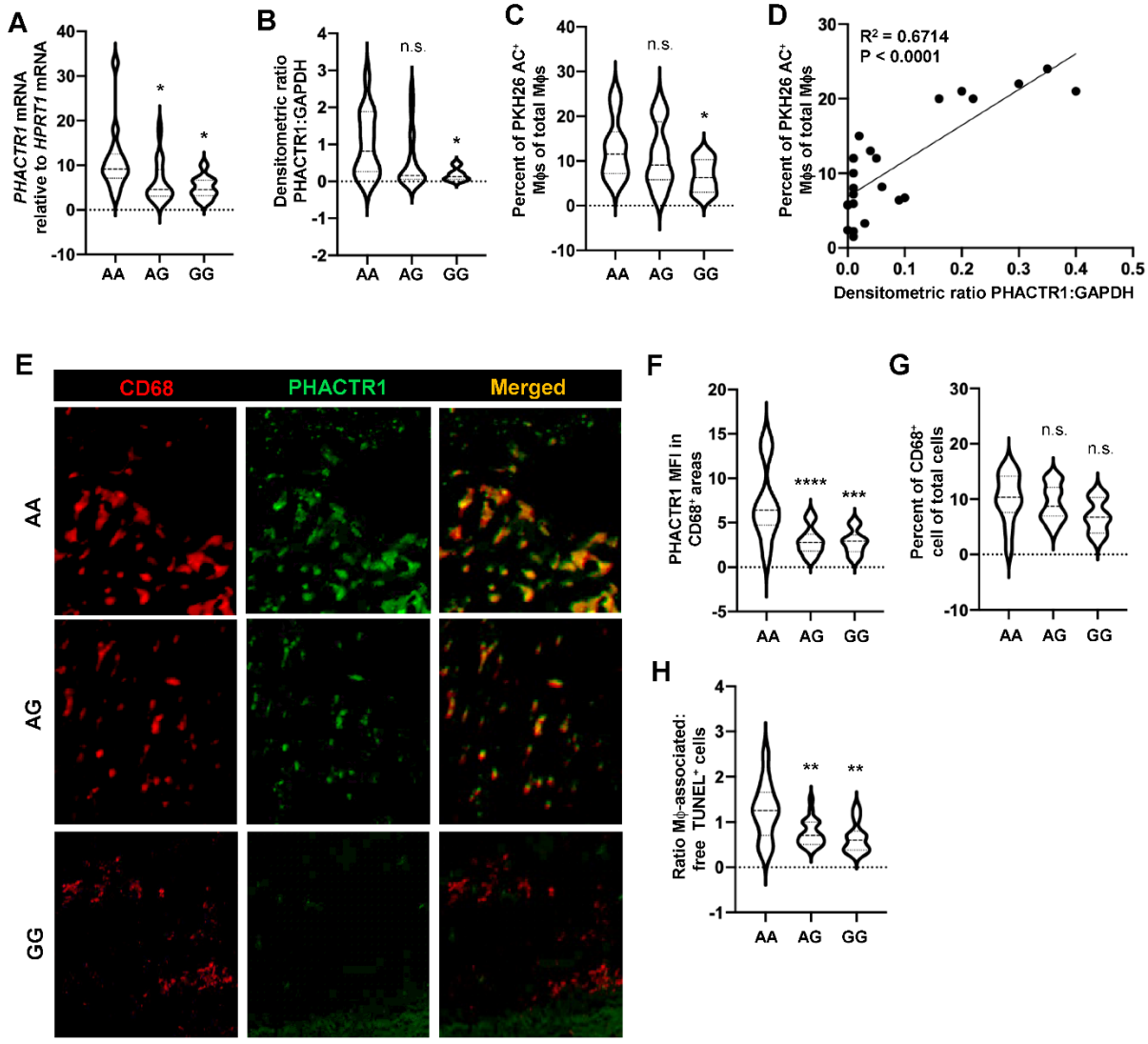

Figure 1. Human monocyte-derived and atherosclerotic lesional macrophages carrying the rs9349379-G CAD-risk variant have lower PHACTR1 expression and impaired efferocytosis. (**A-D**) Human monocyte-derived macrophages (HMDMs) were genotyped for rs9349379 SNP (n = 48; AA = 14, AG = 24, GG = 10) and then assayed as follows: (**A**) relative *PHACTR1* mRNA by qPCR (normalized to HRPT1); (**B**) PHACTR1 protein (~75 kDa) by immunoblot (densitometric ratio with GAPDH (36 kDa) and expressed relative to AA); and (**C**) percent of HMDMs that engulfed PKH26-labeled apoptotic cells (ACs). (**D**) Plot of efferocytosis versus PHACTR1 protein expression of rs9349379-AG HMDMs (r^2 and P-value obtained using Spearman correlation analysis). (**E-H**) Human carotid endarterectomy specimens were genotyped for rs9349379 SNP (n = 45; AA=13, AG=22, GG=10) and then fixed and sectioned for immunofluorescence microscopy. (**E**) Sections were co-stained for PHACTR1, CD68, and DAPI; scale bar, 50 μm. (**F**) The mean fluorescent intensity (MFI) of PHACTR1 in $CD68^+$ areas and (**G**) the percentage of $CD68^+$ cells to total $DAPI^+$ cells was quantified. For each subject, 5 areas were analyzed, and the MFI value was averaged. Sections stained with isotype control antibodies for PHACTR1 and CD68 showed an absence of signal. (**H**) Sections were co-stained with TUNEL and CD68. Each $TUNEL^+$ cell was determined to be either associated with a macrophage or not ("free"), and the data are presented as the ratio of macrophage-associated:free $TUNEL^+$ cells. For panels A-C and E-H, $^*P < 0.05$, $^{**}P < 0.01$, $^{***}P < 0.001$, $^{****}P < 0.0001$ compared with the AA group, using one-way ANOVA with Dunnett's multiple comparisons test; n.s., non-significant.

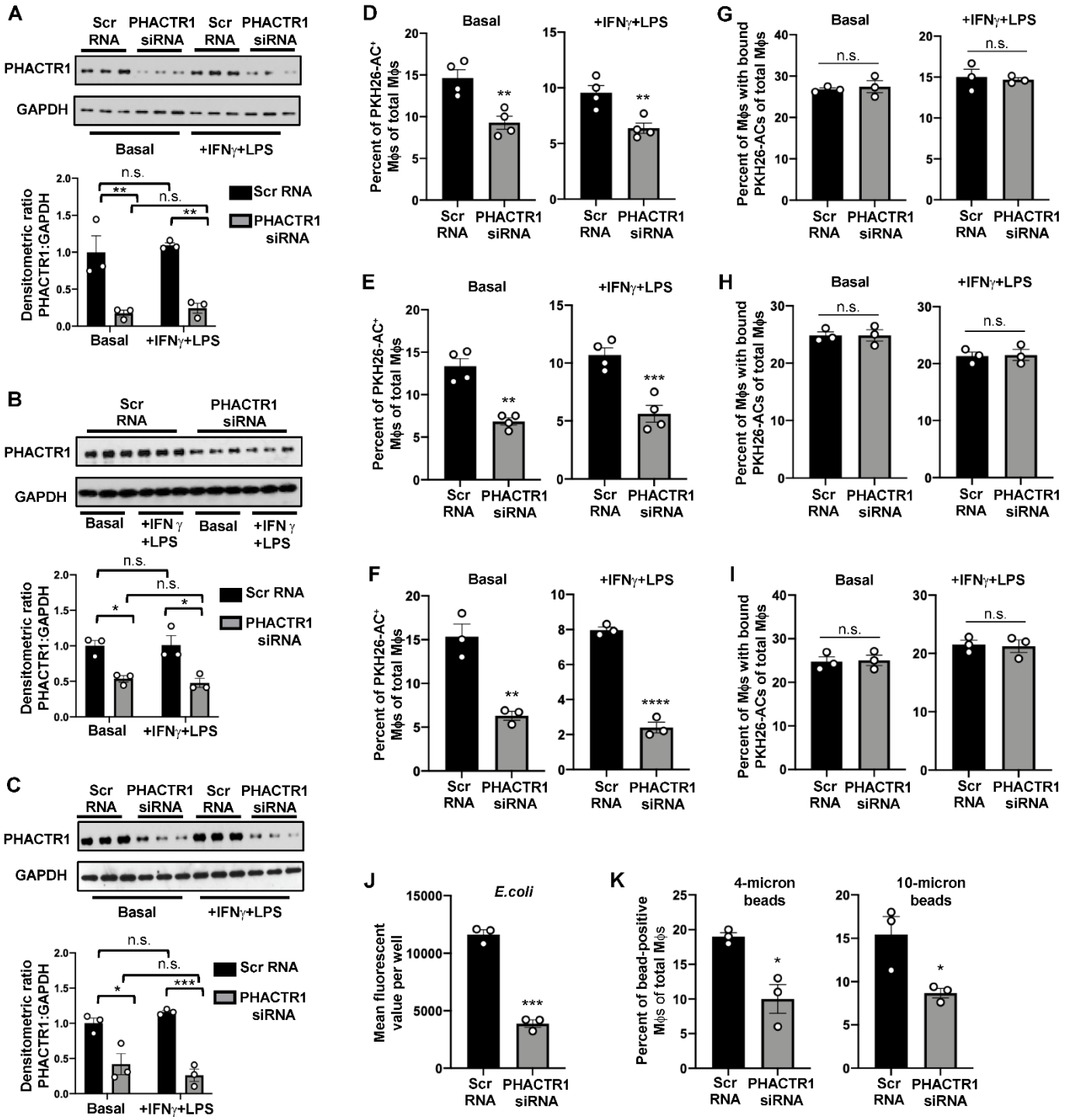

Figure 2. Silencing PHACTR1 in HMDMs decreases efferocytosis and phagocytosis. Human monocyte-derived macrophages (HMDMs) from three of the rs93749379-GG subjects in Fig. 1 were transfected with either scrambled RNA (Scr RNA) or PHACTR1 siRNA. The cells were then incubated with or without interferon-γ (IFNγ) and lipopolysaccharide (LPS). (**A-C**) Immunoblots for PHACTR1 (~75 kDa) and GAPDH (36 kDa) using HMDMs from subjects #1, #2, and #3, respectively, with quantification of densitometric data. Results are shown as mean + SEM; n = 3 experiments; *P < 0.05, **P < 0.01, ***P < 0.001 by 2-way ANOVA with post hoc Tukey's analysis. (**D-F**) Efferocytosis of PKH26-labeled apoptotic cells (ACs) by HMDMs from subjects #1, #2, and #3, respectively. (**G-I**) AC binding to HMDMs from subjects #1, #2, and #3, respectively, pre-treated with 5 μM cytochalasin D for 20 min. (**J-K**) Internalization of *E. coli* and 4-mm and 10-mm polystyrene beads by HMDMs from subject #1. For panels D-K, n = 3 biological replicates, using the average of technical triplicates for each. Results are shown as mean ± SEM, including individual datapoints.*P < 0.05, **P < 0.01, ***P < 0.001, ****P < 0.0001 by unpaired Student's t-test. n.s., non-significant.

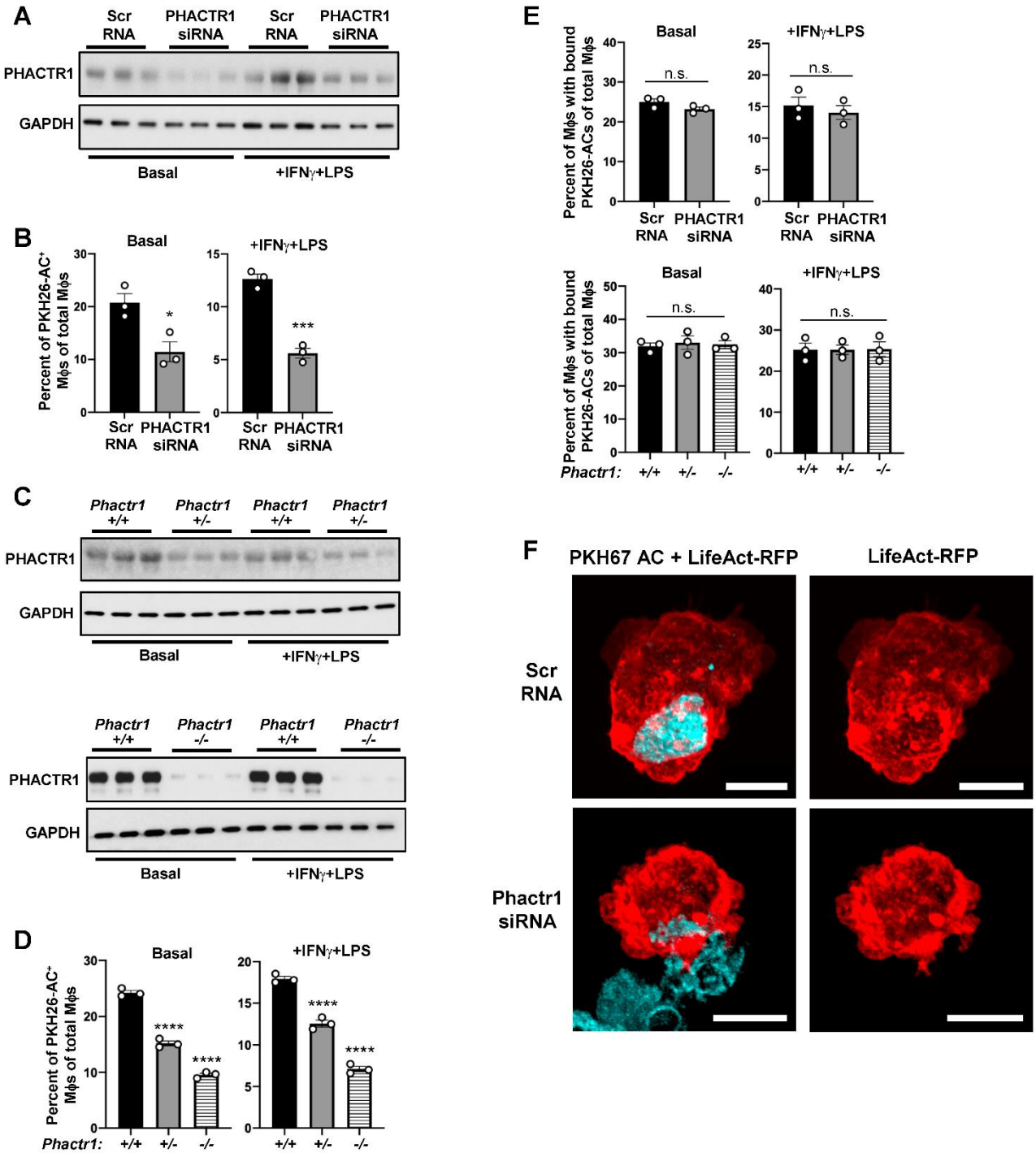

Figure 3. PHACTR1 deficiency impairs phagocytic internalization of apoptotic cells in BMDMs. (**A-D**) Bone marrow-derived macrophages (BMDMs) transfected with either scrambled RNA (Scr RNA) or Phactr1 siRNA (**A-B**), or from *Phactr1*$^{+/+}$, *Phactr1*$^{+/-}$, or *Phactr1*$^{-/-}$ mice (**C-D**), were incubated with or without IFNγ and LPS and then assayed for PHACTR1 protein (~72 kDa) by immunoblot or for efferocytosis. (**E**) BMDMs from A-D were assayed for apoptotic cell binding in the presence of cytochalasin D. (**F**) BMDMs treated with Scr RNA or Phactr1 siRNA were transfected with LifeAct-RFP and then incubated with PKH67-labeled ACs for 45 min. After fixation, the cells were viewed by confocal fluorescence microscopy. Two examples of 0.5-μm z-step images from each group are shown; left, RFP-PKH67-merged channel; right, RFP-only channel; scale bars, 10 μm. For panels B, D, and E, values are mean ± SEM, including individual datapoints; n = 3 experiments. For panel B and upper panel E, *P < 0.05, ***P < 0.001 by unpaired Student's t-test. For panels D and lower panel E, ****P < 0.0001 compared with *Phactr1*$^{+/+}$ by one-way ANOVA with Dunnett's multiple comparisons test. n.s., non-significant.

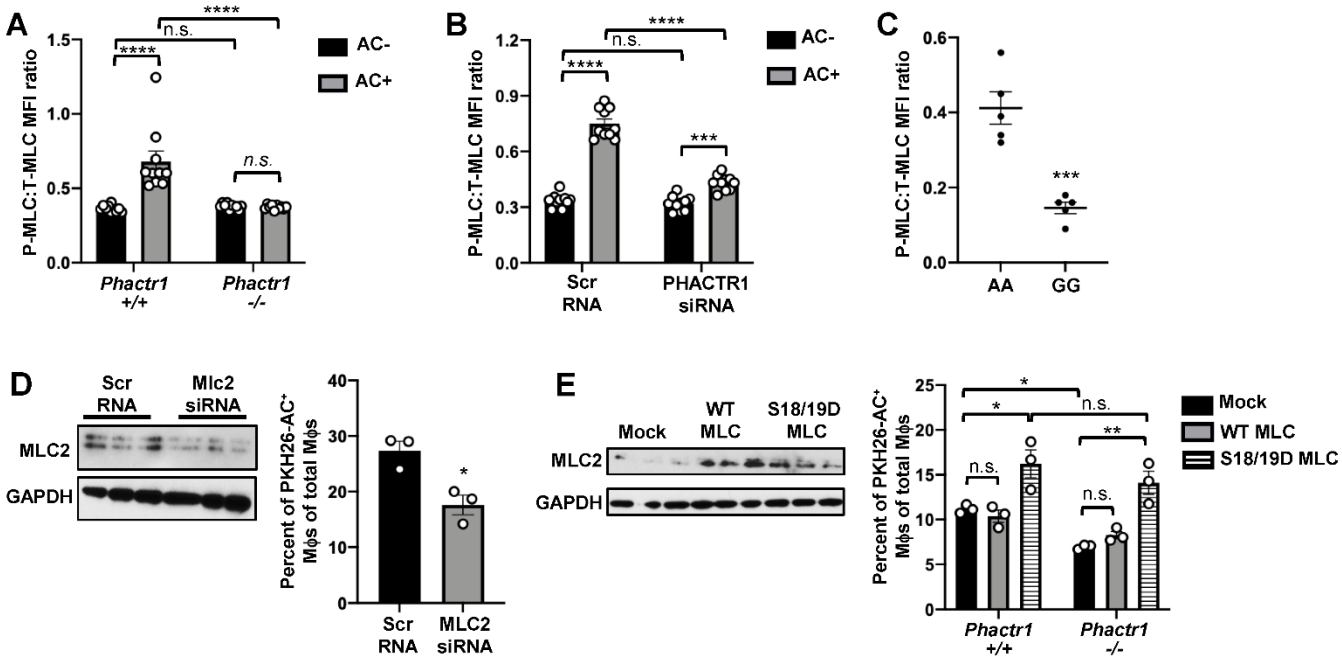

Figure 4. PHACTR1 facilitates efferocytosis by increasing myosin light chain (MLC) phosphorylation. (**A**) Ratio of mean fluorescence intensity (MFI) of phospho (P)-MLC to total (T)-MLC was quantified in *Phactr1*$^{+/+}$ and *Phactr1*$^{-/-}$ BMDMs incubated in the absence or presence of ACs (AC-, AC+). (**B**) HMDMs were treated with scrambled RNA or PHACTR1 siRNA and as assayed for P-MLC:T-MLC MFI ratio as in panel A. (**C**) Ratio of P-MLC to T-MLC was quantified for MFI in AC+ rs9349379 GG and AA HMDMs as in Figure 1. Images were quantified for P-MLC:T-MLC MFI ratio, n = 5 HMDMs per group; $^{***}P < 0.001$ by Student's unpaired t-test. (**D**) BMDMs treated with scrambled RNA or Mlc2 siRNA were then immunoblotted for MLC (18 kDa) and GAPDH (36 kDa) or assayed for efferocytosis. Results are shown as mean + SEM; n = 3 experiments; *P < 0.05 by Student's unpaired t-test. **(E)** *Phactr1*$^{+/+}$ and *Phactr1*$^{-/-}$ BMDMs were transfected with empty vector (Mock) or vector encoding WT MLC or S18/19D MLC. One set of cells was immunoblotted for MLC and GAPDH, and the other was assayed for efferocytosis. Results are shown as mean ± SEM, including individual datapoints; n = 3 experiments; *P < 0.05, **P < 0.01 by 2-way ANOVA with post hoc Tukey's analysis. n.s., non-significant.

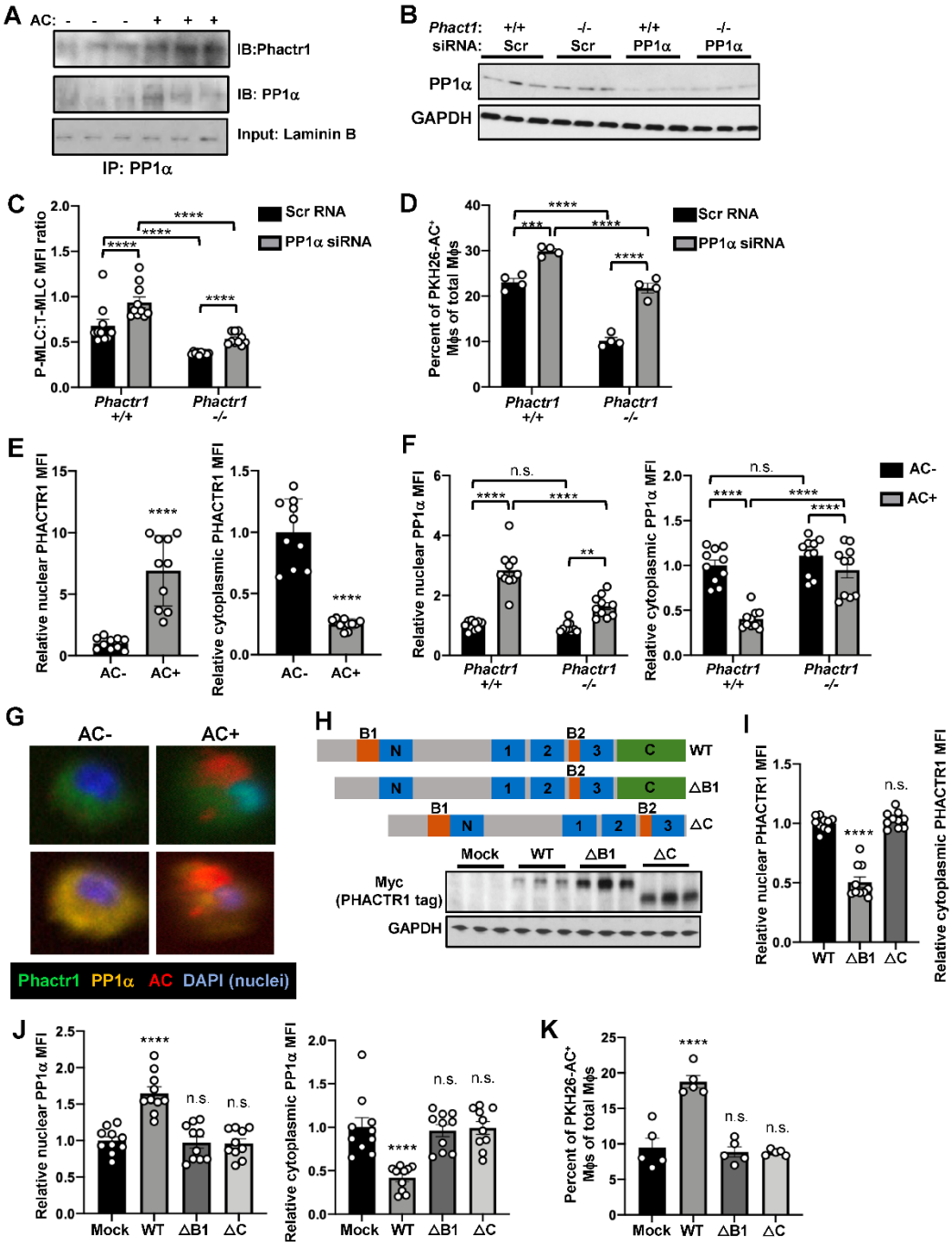

Figure 5. PHACTR1 sequesters PP1α in the nucleus and decreases the dephosphorylation of MLC during efferocytosis. (**A**) Immunoblot of PHACTR1 (~72 kDa), PP1α (38 kDa), and laminin B (input control; 68 kDa) of anti-PP1α immunoprecipitates from BMDMs incubated in the absence or presence of ACs. (**B-D**) *Phactr1*$^{+/+}$ and *Phactr1*$^{-/-}$ BMDMs treated with scrambled RNA or Pp1α siRNA. One set of cells was immunoblotted for PPA1α (38 kDa) and GAPDH (36 kDa), one set was stained with phospho- and total MLC antibody and quantified as phospho:total MLC MFI ratio, and one set was assayed for efferocytosis. (**E**) Quantification of nuclear and cytoplasmic PHACTR1 in BMDMs incubated in the absence or presence of ACs. (**F**) Quantification of nuclear and cytoplasmic PP1α in *Phactr1*$^{+/+}$ and *Phactr1*$^{-/-}$ BMDMs incubated in the absence or presence of ACs. (**G**) Immunofluorescence microscopy images of BMDMs incubated in the absence or presence of ACs (*green*, PHACTR; *yellow*, PP1α; *red*, AC; *blue*, DAPI [nucleus]). (**H**) Graphic scheme of PHACTR1 wild-type and mutant protein structure and immunoblots of Myc (PHACTR1 tag) and GAPDH in *Phactr1*$^{-/-}$ BMDMs transfected with wild-type and mutant PHACTR1 (Myc-tagged PHACTR1 protein is ~73 kDa in WT and ΔB1, and ~70 kDa in ΔC). (**I-K**) Quantification of nuclear and cytoplasmic PHACTR1 and PP1α and efferocytosis in the BMDMs depicted in panel H. For panels C-F and I-K, mean ± SEM, including individual datapoints; n = 3 experiments, with n > 5-10 macrophages quantified for each group; **P < 0.01, ***P < 0.001, ****P < 0.0001 by Student's unpaired t-test (E) or 2-way ANOVA with post hoc Tukey's analysis, compared with WT in panel I and Mock in panels J-K; n.s., non-significant.

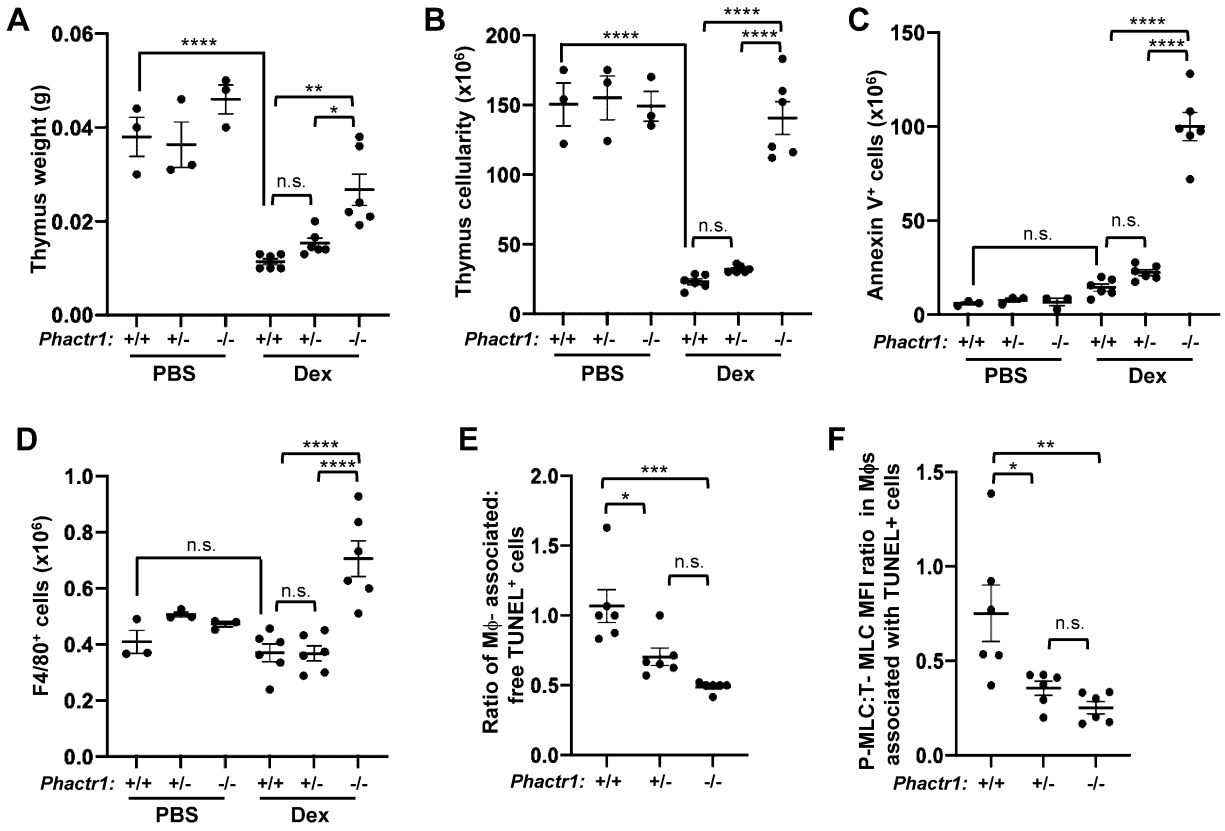

Figure 6. Chimeric mice lacking hematopoietic PHACTR1 show defective macrophage efferocytosis of apoptotic thymocytes. Irradiated mice were transplanted with bone marrow from *Phactr1* $^{+/+}$, *Phactr1*$^{+/-}$, or *Phactr1*$^{-/-}$ mice. After 6 weeks, the mice were injected i.p. with PBS or 250 mg/mouse dexamethasone. After 18 hours, the thymuses were harvested. (**A-D**) Thymic weight, cellularity, and content of annexin V^{+} cells and F4/80^{+} cells. (**E**) Thymus sections were stained for TUNEL and Mac2 and then quantified for the ratio of macrophage-associated:free TUNEL^{+} cells. (**F**) Thymus sections were stained for TUNEL, Mac2, phospho-MLC (P-MLC), and total-MLC (T-MLC), and the ratio of P-MLC to T-MLC was quantified for mean fluorescence intensity (MFI) in macrophages associated with TUNEL^{+} cells. For all panels, results are shown as individual datapoints with lines indicating mean ± SEM; n = 3 mice for PBS groups and n = 6 mice for dexamethasone groups; *P < 0.05, **P < 0.01, ***P < 0.001, and ****P < 0.0001 by one-way ANOVA with Dunnett's multiple comparison test; n.s., non-significant.

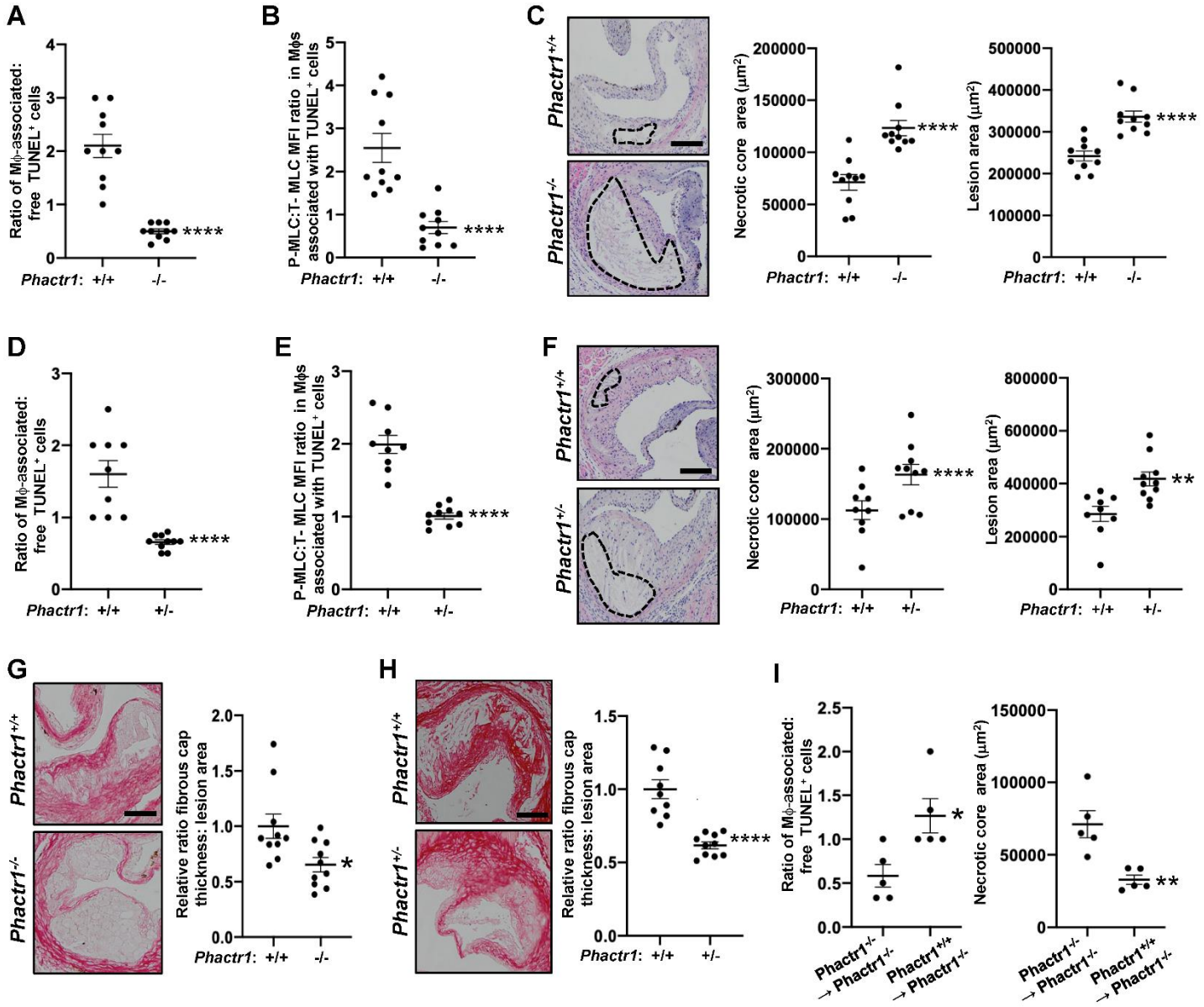

Figure 7. Western diet-fed *Ldlr*$^{-/-}$ mice lacking hematopoietic PHACTR1 show defective macrophage efferocytosis and increased plaque necrosis in atherosclerotic lesions. (**A-C, G**) Irradiated *Ldlr*$^{-/-}$ mice were transplanted with bone marrow from *Phactr1*$^{+/+}$ or *Phactr1*$^{-/-}$ mice. After 4 weeks, the mice were fed a Western-type diet (WD) for 8 weeks, and then aortic root lesional cross-sections were analyzed. (**A**) Ratio of macrophage (Mac2^{+})-associated:free TUNEL^{+} cells. (**B**) Ratio of phospho (P)-MLC to total (T)-MLC mean fluorescence intensity (MFI) in macrophages associated with TUNEL^{+} cells. (**C**) Images of aortic root sections stained with H&E (dashed lines indicate necrotic area [N]), with quantification of necrotic and lesion areas. (**D-F, H**) Irradiated *Ldlr*$^{-/-}$ mice were transplanted with bone marrow from *Phactr1*$^{+/+}$ or *Phactr1*$^{+/-}$ mice. After 4 weeks, the mice were fed the WD for 12 weeks. (**D-F**) Lesional endpoints were quantified as above. (**G, H**) Aortic root cross-sections were stained with picrosirius red. For each section, cap thickness was measured at the lesional midpoint and both shoulder regions and then averaged and quantified as the ratio of collagen cap thickness:lesion area, relative to the *Phactr1*$^{+/+}$ group. (**I**) Irradiated *Phactr1*$^{-/-}$ *Ldlr*$^{-/-}$ mice were transplanted with bone marrow from *Phactr1*$^{-/-}$ *or Phactr1*$^{+/+}$ *mice*. After 4 weeks, the mice were fed a high-fat Western-type diet (WD) for 8 weeks, and lesional endpoints were quantified as above. For all panels, results are shown as individual datapoints with lines indicating mean ± SEM; *P < 0.05, $^{**}P$ < 0.01, $^{****}P$ < 0.0001 by Student's unpaired t-test. n.s., non-significant. Scale bars, 100 μm.